Thin-Walled Structures 184 (2023) 110481

Contents lists available at ScienceDirect

Thin-Walled Structures

journal homepage: www.elsevier.com/locate/tws

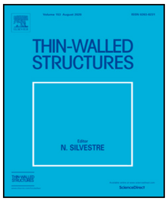

Full length article

Formation of post-buckling shear mechanisms in stiffened web panels of slender steel plate girders

Kevin E. Augustyn [a], Spencer E. Quiel [a,*], Maria E.M. Garlock [b]

[a] Department of Civil and Environmental Engineering, Lehigh University, Bethlehem, PA, United States of America
[b] Department of Civil and Environmental Engineering, Princeton University, Princeton, NJ, United States of America

ARTICLE INFO

Keywords:
Web shear buckling
Slender steel plate girder
Ultimate shear resistance
Shear mechanisms
Second-order plate bending
Tension field action

ABSTRACT

A series of validated finite element models are used to investigate the formation of mechanisms in stiffened slender web panels of steel plate girders under pure shear. The prototype girder is based on the seminal tests by Basler and has a web slenderness of 267. Six model cases are analyzed with variations in web panel aspect ratio (1, 1.5, and 3), steel yield strength (Grades 36 and 50), initial imperfection magnitude, and flange thickness. When loaded in shear, the web panels exhibit a 3-stage response: (1) elastic behavior, (2) web mechanism formation, and (3) panel mechanism. In Stage 1, the web initially exhibits an elastic in-plane shear response with no distinct buckling bifurcation. During this stage, the web's initial out-of-plane imperfections become engaged in second-order bending along its compression diagonal. Concurrently, tension develops in the opposite diagonal as a non-uniform membrane stress field, with highest intensities at locations where second-order bending is low. In Stage 2, a web mechanism is formed when connected bands of thru-thickness von Mises yielding develop across the tension diagonal. These bands emerge at locations where tension membrane stresses interact with locations of maximum second-order bending stress in the buckled shape. The shear load at the end of web mechanism formation is recommended as a target for plastic limit state design because it marks a significant decrease in shear stiffness. In Stage 3, von Mises yielding continues to saturate the web panel, and the bounding flanges and transverse stiffeners become increasingly engaged in load redistribution from the plastified web. Any hardening increase in shear resistance during the panel mechanism stage is modest in magnitude (up to ~10% for some cases in this study) and is heavily dependent on the sizing of the flanges and stiffeners to carry redistributed forces.

1. Introduction

The design of long-span I-shaped steel plate girders is often governed by the shear capacity of their slender webs, which are fabricated with thin plates to minimize self-weight and maximum separation (and thus flexural capacity and stiffness contribution) from the flanges. To enhance their shear resistance, the webs are typically stiffened out-of-plane with intermediate transverse stiffener plates that are welded to the web on both sides and span vertically between the flanges (to which they are usually welded as well). The shear behavior of these webs has been studied extensively via testing and numerical analysis for more than 75 years [1], leading to the development of several design models for predicting their shear capacity [2–4]. When the spacing of transverse stiffeners [a (m)] is less than three-times the depth of the web between the flanges [h (m)], the web would be expected to buckle out-of-plane as shear loading increases and eventually develop a collapse mechanism at which the maximum shear resistance is reached. As the web begins to buckle, the initial ideal shear stress profile (i.e. with 45° orientation of the principal stresses, as shown in Fig. 1a) throughout the web gives way to the development of opposing diagonals of tension and compression [4] which are braced by the stiffeners and flanges. As the in-plane and out-of-plane deformations continue to increase, the mode of mechanism formation in these stiffened web panels will determine the maximum resistance that can be developed.

The tension diagonal (or "tension field action") is the centerpiece of most modern steel design codes for civil infrastructure [5–7] and has often been considered in the research literature to be the more significant post-buckling load path toward maximum shear resistance versus the compression diagonal [1]. In fact, the three models upon which modern design specifications are based [8–10] all assume that the tension field in the web is engaged as a planar element, thus neglecting the influence of the compression diagonal and its associated out-of-plane deformations due to second-order bending of the buckled shape. To achieve equilibrium, those models instead utilize other load paths as illustrated in Fig. 1b–d.

---

[*] Corresponding author.
E-mail address: squiel@lehigh.edu (S.E. Quiel).

https://doi.org/10.1016/j.tws.2022.110481
Received 26 July 2022; Received in revised form 15 December 2022; Accepted 16 December 2022
Available online xxxx

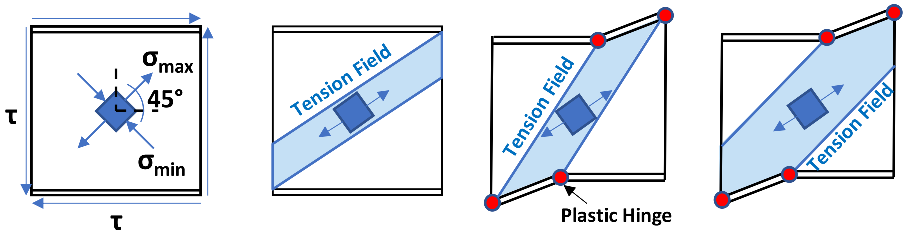

(a) Pre-buckling *(b) Basler [8]* *(c) Höglund [9]* *(d) Cardiff [10]*

Fig. 1. Prominent tension field theories for stiffened slender webs in plate girders under pure shear.

- *The transverse stiffeners are engaged in axial compression*, thus emulating a Pratt truss with the flanges as the chords and the web tension field as the diagonal (i.e. Basler's model [8], which the basis of current North American design practice for shear resistance of slender plate girders in buildings [5] and bridges [6]). A mechanism would be formed when the web tension diagonal reaches yield. Basler's model (Fig. 1b) assumes that the flanges too flexible to participate in the development of post-buckling shear strength via weak-axis bending.
- *The flanges are engaged in weak-axis flexure*, thus directly anchoring the tension field until the formation of an ultimate shear mechanism when the web tension field activates four flexural hinges in the flanges, located at the corners of the tension field as shown in Fig. 1c (i.e. Höglund's rotated stress model [9], which is the basis for calculating shear resistance in slender plated structures per Eurocode 3, Part 1–5 [7]). The principal stresses in the buckled web become "rotated" to be flatter than 45° because the tension diagonal stresses increase faster than the compression diagonal stresses. The resulting rotated-stress theory posits that the maximum web shear strength can be calculated by applying a reduction factor (representing the rotated field) to the web's shear yield resistance, plus the flexural resistance of the flanges.
- *Both of the axial-stiffener and flexural-flange load paths are engaged together*, and a mechanism in the web panel would again occur when four flexural plastic hinges formed in the flanges of a panel after the tension field in the web yielded. The so-called Cardiff model [10] (Fig. 1d) is considered to be a more comprehensive prediction of post-buckling web shear resistance but with increased calculational complexity versus those by Basler or Höglund [2]. It should be noted that when the flexural contribution of the flanges are considered to be negligible, then the Cardiff model reduces to be mechanically equivalent to the Basler model [1,2].

Recent research has shown that the load path through the stiffeners contribute much less to the formation of a mechanism than the behavior of the buckled web itself. Numerous studies (among them [4,11–18]) have repeatedly demonstrated that the magnitude of axial compression in the transverse stiffeners up to maximum shear strength is well below that which would emulate the verticals in a Pratt truss. In its 2016 edition, Section C-G2-3 in the commentary of AISC 360-16 *Specification for Structural Steel Buildings* [5] now acknowledges the low axial compression in the transverse stiffeners and explicitly references the aforementioned studies and others. Instead, Section C-G2-2 of AISC 360-16 posits that the compression vertical of the effective Pratt truss is established in the web where it is braced by the stiffener. However, Augustyn et al. [11] showed via numerical analyses that the axial compression in these web regions was similar to that in the stiffeners and, again, much less than would be expected in a Pratt truss emulation.

Recent studies have also shown that flexural flange engagement as anchorage for the tension field has little impact on the development of the plastic web panel mechanism [17,18], and flexural yielding in the flange often occurs after maximum shear is reached [12]. Via numerical analysis, Augustyn et al. [11] showed that an increase in flange thickness has only a marginal influence on the development of a plastic web panel mechanism by providing greater torsional and out-of-plane stiffness to the panel edges. The same increases in flange thickness can be used to enhance the behavior of the panel after the web has fully yielded, which is consistent with the assumptions of both the Höglund [9] and Cardiff models [10]; however, the additional shear resistance achieved by this flange-assisted hardening is only 5%–15% greater than the shear at full web yielding.

Without significant pre-mechanism contributions from the axial-stiffener and flexural-flange load paths, the compression diagonal in the web would therefore be needed to establish equilibrium up to the point at which the web reaches thru-thickness yielding [11]. The deformed compression diagonal would thereby develop a spring-like load path with associated stiffness and strength — these compression-driven mechanics formed the basis of the web-shear buckling theory by Timoshenko and Gere [19] (which did not account for tension field action) and the development subsequent compression-based web shear buckling models by Glassman and Garlock [4] (which did incorporate aspects of tension field action). Experimental [20] and numerical [21] research by Lee & Yoo has indicated that thru-thickness yielding in the buckled web will be heavily influenced by second-order bending stresses in the out-of-plane deformations of the buckled web in the compression diagonal. Both Wang et al. [12] and Garlock et al. [22] used numerical modeling to show that stresses along the compression diagonal will continue to increase (albeit at rate that decreases as shear loading increases) up to point of thru-thickness web yielding. Specifically, the yielded state is caused by a thru-thickness saturation of von Mises stresses with contributions from both the tension field and second-order compression-induced bending [22].

Despite the extensive research attention over the past 75 years [1], there continues to be a need for a unified consensus theory that accounts for the interaction between the tensile membrane stresses in the tension diagonal and the second-order bending stresses of the buckled web plate in the compression diagonal. To contribute to the evolution of plastic design for slender stiffened web panels under shear loading, this study uses finite element (FE) analyses (validated previously by Augustyn et al. [11]) based on the seminal tests by Basler et al. [23,24] to investigate the formation of shear mechanisms for web panels with aspect ratios (a/h) ranging from 1 to 3 (which are expected to develop tension field action [12]). The web shear mechanics will be defined by these mechanisms, specifically (1) a "web mechanism" described by first yield on the web surface, followed by full thru-thickness yielding across the tension field diagonal where second-order bending stresses are greatest, and (2) a subsequent "panel mechanism" that engages and then overwhelms the flanges and stiffeners as load anchorage pathways. The significant role of second-order bending stresses will also be examined by contrasting the membrane response of the web (which, again, is the focus of the Basler [8], Höglund [9] and Cardiff models [10]) with the combined interaction of second-order bending stresses and the tension field toward a von Mises yield condition [22].

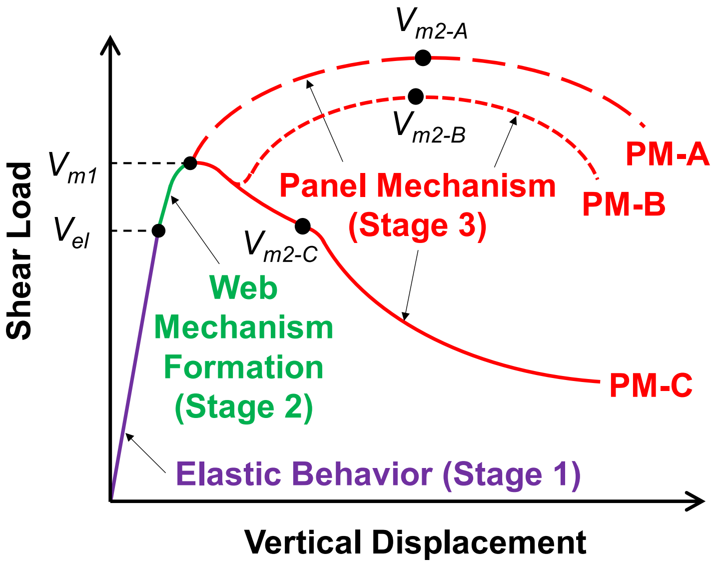

Fig. 2. Generalized shear response for a stiffened slender web panel that experiences shear buckling.

2. Generalized shear response

The existing research literature includes the results of almost 200 shear tests on slender plate girders, and the shear resistances reported from the results have been used extensively to assess the accuracy of the various aforementioned prediction models that are used in current practice [1–3]. Based on the shear load–displacement behavior recorded during many of those tests [20,24–29], Scandella et al. [29] observed three consistent stages of response, which have been adapted for this study as illustrated in Fig. 2: (1) elastic behavior, (2) web mechanism formation (following the first onset of yielding across the web's tension diagonal), and (3) panel mechanism (following the onset of full thru-thickness yielding across the web's tension diagonal). Note that the nomenclature of the stages has evolved from the authors' previous work [11] to more clearly define the stages in terms of the mechanisms described in this paper. A full description of each stage and their transition milestones is provided in the subsections below, and this generalized characterization will be used as the basis for evaluating the results of all FE analyses in this study.

2.1. Stage 1: Elastic behavior

The shear load–displacement reported from numerous experimental tests [20,24–29] have all shown an initially elastic relationship before reaching an elastic limit. None of these studies showed any indication of a sudden change of stiffness or a buckling bifurcation point during the initial load–displacement response. The web panel does not experience sudden buckling because it is not perfectly flat in its initial state, and the initial imperfections are engaged in second-order compression-induced bending throughout the elastic stage. The out-of-plane deformations will settle into a stable shape and progressively increase as in-plane shear loading increases [11]. As a result, the in-plane shear resistance of the stiffened web panel will be elastic but semi-linear due to the onset of second-order bending in the initially deformed shape. Specifically, the in-plane shear stiffness will decrease slightly as out-of-plane deformations increase and the plate becomes more "buckled". During the elastic stage, the principal membrane stress angles will become progressively flatter (i.e. less than 45°) toward the end of the elastic stage as tension and compression diagonals become more pronounced and out-of-plane bulging deformations increase via compression-induced second-order bending. The critical elastic buckling shear load, V_{cr}, occurs during this stage but is not a physically significant milestone for reasons described in the next subsection.

2.2. Elastic limit milestone: V_{el}

The first transition milestone, elastic limit V_{el}, is reached when the tensile stresses along the tension diagonal interact with the compression-induced second-order bending stresses to produce a von Mises yield condition on the surface of the web plate. At V_{el}, this surface yield condition is now fully connected across the tension field diagonal and emerges where tensile stresses are largest due to second-order bending (i.e. at the outer surface of the largest "bulge" of out-of-plane deformation). This milestone is marked by a sudden change in the in-plane shear stiffness, which can be directly observed by calculating the second derivative of the shear load–displacement curve in Fig. 2. Previous numerical studies on these girders by the authors [11] indicated that there is no demonstrable increase in either stiffener engagement (via axial compression) or flange anchorage (via weak axis bending) at this milestone.

It is important to note that V_{el} is not equivalent to V_{cr}, which is obtained from eigenvalue buckling analysis of a perfectly flat web plate and therefore has little physical meaning for a plate with realistic initial out-of-plane imperfections. Wang et al. [12] conducted numerical analyses of stiffened web panels with initial imperfections based on the first eigenmode shape and with maximum scaled magnitude varying from $h/100$ to $h/10{,}000$. The results showed somewhat of a bifurcation at $h/10{,}000$, which is "nearly flat" and much smaller than realistic web imperfections in actual girders [30]. More realistic imperfection magnitudes ranging from $h/1000$ to $h/100$ (the latter of which is used for this study based on prior validation [11]) showed no clear bifurcation and instead showed a quasi-linear onset of web shear response during the elastic stage (very similar to shear load–displacement relationships in the experimental literature [20,24–29]). The lack of a consistent and distinct web shear buckling bifurcation indicates that V_{cr} (as a purely theoretical value based on analysis of an ideally flat web) is only meaningful for developing initial imperfection patterns for numerical analysis.

2.3. Stage 2: Web mechanism formation

In their 3-stage characterization of web shear load–displacement behavior, Scandella et al. [29] had referred to the second and third stages as "post-buckling" stages. Due to the lack of a clear buckling bifurcation when realistic initial imperfections are considered, this study renames Stages 2 and 3 to more aptly identify the true mechanical response of the buckled web after its shear load exceeds V_{el}. Beyond that point, the in-plane shear stiffness (i.e. the first derivative of the shear load–displacement curve in Fig. 2) will progressively decrease through Stage 2 as the surface yield condition begins to saturate (i.e. penetrate) through the full thickness of the web plate across the tension field diagonal where compression-induced second-order bending stresses are high. The stiffener and flange anchorage load paths are not significantly engaged until after the web mechanism is fully developed [11], and the web therefore continues to provide the majority of the shear resistance during the web mechanism formation stage.

2.4. Web mechanism milestone: V_{m1}

At the end of Stage 2, the web across the tension diagonal has achieved thru-thickness von Mises yielding due to the increasing stress interaction between maximum second-order bending locations and the tension field. Milestone V_{m1} thereby represents the formation of the web mechanism and is marked by another sudden change in the in-plane shear stiffness. Beyond V_{m1}, the shear stiffness of the web panel will begin to decrease as the tension field diagonal load path has now fully yielded.

2.5. Stage 3: Panel mechanism

Following the formation of the web mechanism, the plastified web panel will increasingly engage the flanges and stiffeners, which now offer relatively stiff load paths to support shear load redistribution as in-plane shear displacement progresses at an increasing rate. Load redistribution to these supporting elements will eventually cause a panel mechanism to develop at shear load V_{m2} when the load paths to those elements yield or become unstable. Beyond V_{m2}, the shear resistance of the stiffened web panel will proceed along a descending branch toward collapse. This sequence of load path engagement has been observed in numerous prior studies (including [9,11,15,17,21]) and can influence the shape of the shear displacement response during the panel mechanism stage as shown in Fig. 2. Regardless of the shape of the Stage 3 curve, all girders will experience a small but non-negligible recovery in stiffness as the load redistribution pathways become fully engaged after exceeding V_{m1}. The shape of the Stage 3 shear load–displacement curves will depend on the degree of support provided to the plastified web by those boundary elements:

- ***PM-A***: The shear resistance continues to increase but at a reduced rate (i.e. positive hardening) after the web's tension diagonal undergoes thru-thickness yielding at V_{m1}. This immediate transition to mechanical hardening is enabled by load redistribution to flanges that are large enough to adequately anchor the web mechanism [9–11] and/or very stiff transverse stiffeners that can act as vertical struts [17]. Maximum shear resistance is reached once a second mechanism is developed at $V_{m2\text{-}A}$ (see Fig. 2), beyond which the web panel enters a descending branch toward collapse.
- ***PM-B***: The overall shear resistance trajectory is similar to PM-A but initially dips to a local valley following the formation of the web mechanism at V_{m1}. The load redistribution pathways to the flanges and stiffeners then become fully engaged, enabling positive hardening to a subsequent peak of shear resistance when a second mechanism is formed at $V_{m2\text{-}B}$. Note that the value of $V_{m2\text{-}B}$ may or may not exceed V_{m1} depending on the stiffness provided by the load redistribution pathways. For the representative example in Fig. 2, maximum shear resistance is reached at $V_{m2\text{-}B}$ due to hardening recovery following the formation of the web mechanism.
- ***PM-C***: The plastified web panel will yet again engage the aforementioned load redistribution pathways and develop a panel mechanism $V_{m2\text{-}C}$; however, the boundary elements are unable to support any subsequent hardening increase in shear resistance past V_{m1}. Therefore, maximum shear resistance is essentially equivalent to V_{m1} as shown in Fig. 2, after which the shear resistance gradually descends until the development of the panel mechanism at $V_{m2\text{-}C}$. Beyond $V_{m2\text{-}C}$, the slope of the descending branch becomes increasingly negative toward collapse.

2.6. Commentary on maximum vs. ultimate shear

Note that Fig. 2 and the associated discussion in Sections 2.1 through 2.5 do not utilize the term "ultimate shear" to describe any of the shear mechanism milestones. Most existing predictions of post-buckling web shear capacity (including those by Basler [8], Höglund [9], and Porter et al. [10]) commonly use the term ultimate to denote the state of maximum shear as a target for design. In that context, ultimate shear load would be synonymous with the peak or maximum shear load regardless of the mechanism(s) that preceded it, as suggested by Lee & Yoo [20]. Alternatively, Scandella et al. [29] explicitly defined the ultimate shear load at the formation of the panel mechanism (similar to V_{m2} per the nomenclature in this study), at which the descending branch initiates toward shear failure. In that context, the ultimate shear value may or may not exceed the shear load achieved at the earlier formation of the web mechanism (i.e. V_{m1} per this study).

In their review of numerous prediction methods for post-buckling web shear resistance, White & Barker [2] used "maximum shear resistance" rather than the term "ultimate" to denote peak shear capacity, thus recognizing that different prediction methods (and the test results from which they were developed) used different mechanism milestones to describe that state. For example, the seminal G7 test by Basler et al. [24] demonstrated a PM-C shear-displacement response per Fig. 2 and achieved maximum shear resistance at the formation of the web mechanism (at relatively small shear displacement). Numerous web shear tests by Rockey and Skaloud [25,31], Lee & Yoo [20], and Hansen [28] demonstrated a PM-A response per Fig. 2 and achieved maximum shear resistance during the formation of the panel mechanism (at much larger shear displacement). Recent tests by Scandella et al. [29] demonstrated a PM-B response per Fig. 2 and developed maximum shear resistance at the formation of either mechanism depending on the configuration of the web panel, flanges, and stiffeners. The results of these tests and others [1] have shown that the shape of the Stage 3 Panel Mechanism response is a product of the web panel boundary conditions, as will be further demonstrated by the numerical results of this study. To avoid confusion regarding the definition of the "ultimate" shear state, this study instead uses V_{m1} and V_{m2} to specifically identify the formation of the web and panel mechanisms, respectively. Also, the term "maximum shear resistance" will be used per White & Barker [2] to denote the peak load achieved at any point in the shear-displacement response.

3. Numerical study

3.1. Plate girder prototypes

The prototype plate girder used for this study is based on specimens G6 and G7 that were tested by Basler et al. [23,24] for pure shear loading. Fig. 3 shows the geometry, support conditions, and load application locations for the prototype girder, which has a web slenderness (equal to h, the clear distance between the flanges, divided by t_w, the web thickness) of 267, The value of h equals 1270 mm for all specimens and is marked in Fig. 3. This setup concentrates shear buckling behavior within the central "test section", which has a thinner 4.76-mm (3/16-in) web plate and develops constant shear with minimal moment per Fig. 3. The transition between web thicknesses was made via a welded butt joint at 304.8 mm beyond the extent of the test section to provide web-shear continuity. Welded intermediate stiffeners are equally spaced across the length of the test section to create a desired web panel aspect ratio, calculated as a/h where a is the panel length. Each stiffener location for these girders has a symmetric

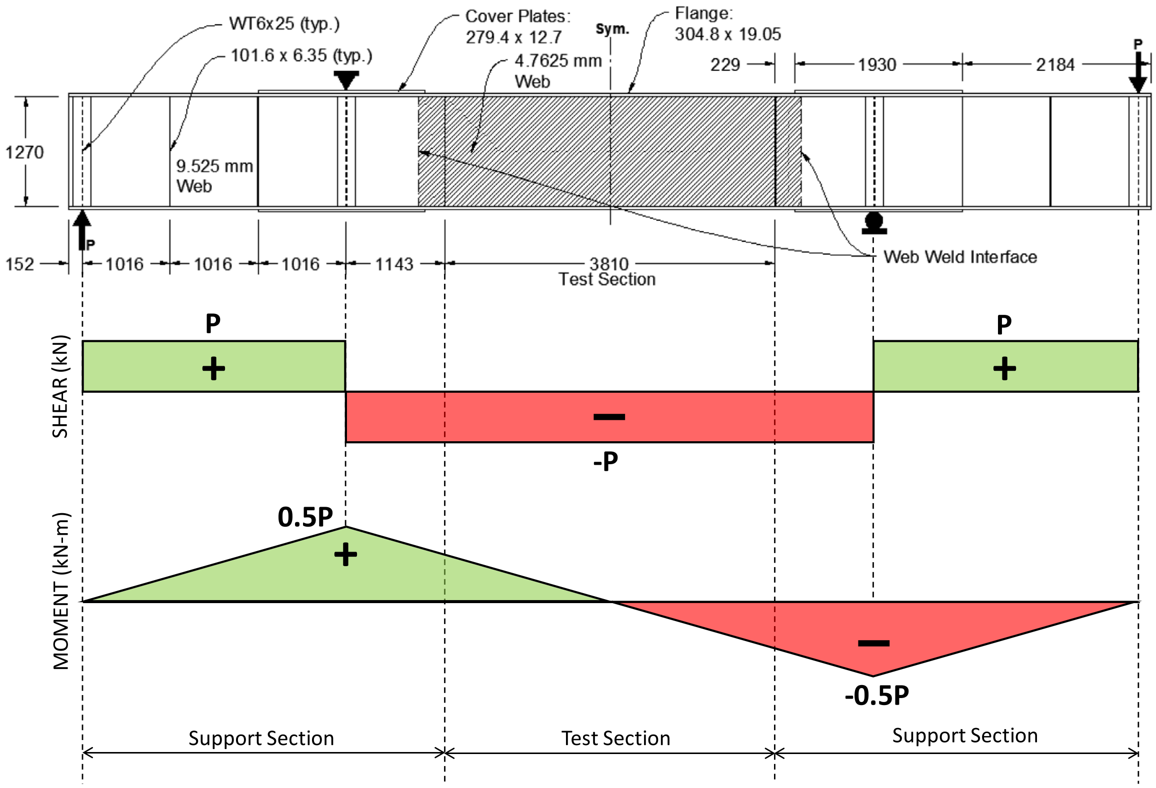

Fig. 3. Prototype plate girder and test setup per Basler et al. [23] (shown here with $a/h = 3$ over the test section).

pair of plates (with 101.6 mm transverse width and 6.35 mm thickness over the full depth of the web) on both sides of the web. Three aspect ratios are considered for this study: $a/h = 1$ (using four stiffeners to represent Basler et al.'s G7 specimen [24]), $a/h = 1.5$ (with three stiffeners to represent Basler et al.'s G6 specimen [24]), and $a/h = 3$ (with only two stiffeners, one at each end of the test section).

3.2. Finite element model description

The FE analysis approach used to model these girders (the details of which are described below) was previously validated by the authors [11] against Basler et al.'s test results for the G7 ($a/h = 1$) and G6 ($a/h = 1.5$) specimens [23,24] and demonstrated very close agreement in shear load–displacement behavior. Basler et al.'s test program did not include a girder case with $a/h = 3$ (which is illustrated in Fig. 3); however, the authors [11] also validated the FE analysis approach against test results by Hansen [28] (who utilized a very similar test setup as Basler et al.) for a similarly slender plate girder with a/h equal to 2 and 4. The modeling approach described herein is therefore capable of capturing the full web shear buckling response for all three test section aspect ratios that are considered in this study.

The webs of Basler et al.'s G6 and G7 specimens were fabricated using ASTM A373-56T ("Gr36") steel plate, and the results of their tensile coupon tests [23] were used to develop the true stress–strain relationship used for all steel plates in the FE models [11]. For comparison, the true stress–strain relationship for Basler et al.'s Gr36 steel plates is plotted in Fig. 4 against the true stress–strain for ASTM A709 ("Gr50") steel plate (which is used in steel plate girders for modern bridges) per Brnic et al. [32]. Based on these curves, the actual yield strengths of the Gr36 and Gr50 steel materials are 275 MPa (39.8 ksi) and 386 MPa (56 ksi), respectively.

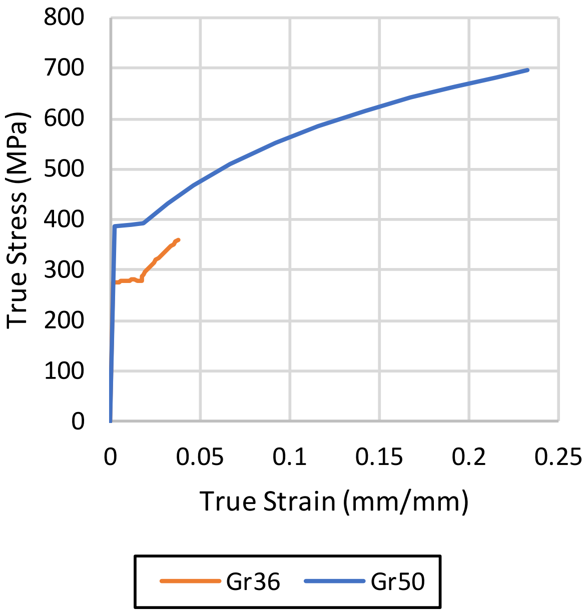

Fig. 4. True stress–strain relationships of steel material input for FE analysis: Gr36 [23] and Gr50 [32].

The girders are modeled in Abaqus 2020 [33] using S4R shell elements (with 7 integration points per the Simpson integration rule through their thickness) that are discretized to maximum edge dimension of 25.4 mm as shown in Fig. 5 (i.e. the web has 50 elements over its depth). Welded joints between plates are modeled by applying a tie constraint between all degrees of freedom at co-located nodes. The vertical extent of the web elements is set equal to the web depth h between the interior flange faces. For simplification, the flange element nodes are placed at $\pm h/2$ from the longitudinal mid-height centerline of the web. The on-center separation between the top and bottom flange elements is therefore reduced from $h + t_f$ to h in the FE models versus the schematics in Fig. 3. Previous work by the authors [11] showed that

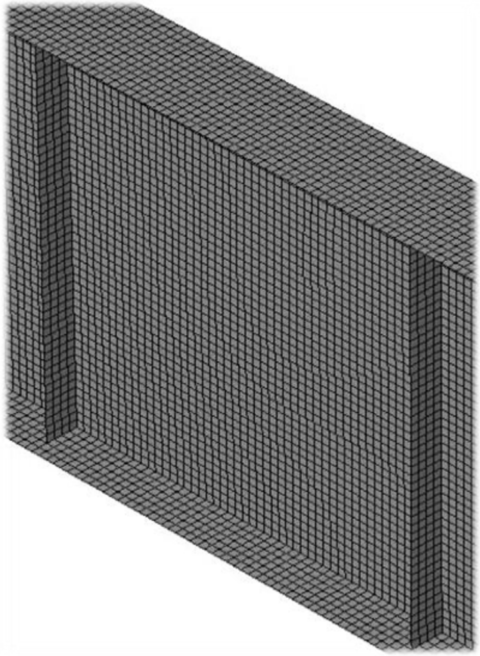

Fig. 5. Isometric view of a discretized web panel in the test section of the prototype girder with $a/h = 1$.

this modeling simplification had negligible impact on the web shear response of the FE model versus Basler et al.'s test results due to the low bending moment in the test section as shown in Fig. 3.

All stiffeners in this study are modeled as fully welded to both flanges and the web, which is representative of current practice [5,6]. It should be noted that the intermediate stiffeners in the test sections of the original Basler et al. G6 and G7 specimens were only welded to the web and to the compression flange, with a 25.4-mm gap between the end of the stiffener and the inside face of tension flange. That gap was representative of plate girder construction practice at the time [23]; however, previous FE modeling by the authors [11] of both the as-built case with the gap and the case with the fully welded stiffener showed practically identical shear load–displacement response.

Basler et al.'s experimental tests [24] applied vertical load (P) via displacement control at the two marked locations in Fig. 3, and vertical displacements were measured at the flange opposite of the load application. The same approach to load application and displacement measurement will be used for all numerical models of the prototype girder in this study. For simplicity, the vertical loads at each end of the girder were applied as a point load to a single node at the intersection of the bearing stiffener, web, and flange. All boundary conditions were applied to a single line of nodes across the full width of the flange at the applicable location. Out-of-plane (i.e. transverse) translation was restrained only at the locations of load application and vertical support. FE analysis of each prototype girder case is performed via numerically stabilized quasi-static loading via the Modified Riks analysis in Abaqus [34] to obtain the full web shear response of the girder to the onset of a collapse mechanism.

3.3. Initial out-of-plane web imperfections

Each girder model has initial imperfections that are imposed onto its geometry prior to performing the Modified Riks analysis. To obtain the imperfection shape, preliminary analysis is performed with ideal geometry (i.e. flat web and no imperfections) via the "buckle" function in Abaqus to obtain the eigenmode shapes for each aspect ratio case. The load at which the first positive eigenmode is achieved is designated as the elastic or critical buckling load, V_{cr}. The shape of the first eigenmode is then scaled relative to a predefined maximum amplitude and imposed onto the initially undeformed girder geometry as an initial imperfection. Note that the thin web plate in the test section exhibits the overwhelming majority of the first eigenmode displacements versus all other plates due to its susceptibility to buckling. The maximum imperfection magnitudes discussed herein are therefore located within the test section web.

A peak initial imperfection magnitude of $h/100$ emulates the maximum out-of-plane web imperfection allowed by current design standards [6,7]. The $h/100$ imperfection magnitude has been commonly used for FE modeling in previous studies on this topic [35,36] as an upper bound value for initial out-of-flatness of a built-up plate girder in practice. Previous FE modeling by the authors [11] was able to closely predict experimental shear load–displacement behavior from tests by Basler et al. [24] and Hansen [28] when the first eigenmode shape was scaled to an initial imperfection amplitude of *h/100*. In those models, all residual stresses due to welding at the web-to-flange interfaces were neglected for simplification, similar to previous numerical studies by others [12,21,35]. The implementation of the scaled first eigenmode shape is based on previous work by Johansson and Veljkovic [37], which validated FE models for steel plated elements that experienced various modes of buckling. Fig. 6 plots the contour of initial out-of-plane imperfections in the web test section for the first eigenmode scaled to $h/100$ for the prototype girder configuration in Fig. 3 with web panel aspect ratio *a/h* varying from 1 to 3. These contours are used as the initial conditions for all analyses in this study unless otherwise noted, and residual stresses are neglected for simplification.

3.4. Model cases

Six model cases are analyzed in this study to examine the parametric web-shear response of the prototype girder. These models are divided equally into two groups, which will be addressed in separate subsequent sections of this paper:

- GROUP 1: Prototype girder using all dimensions per Fig. 3 and Gr36 steel with varying aspect ratio (*a/h* equal to 1, 1.5, and 3) to evaluate the influence of web panel length on web-shear response
- GROUP 2: Prototype girder per Fig. 3 with aspect ratio *a/h* = 1 but with the following variations, to evaluate their impact on web mechanism formation:
    - Reduce the maximum initial imperfection magnitude from $h/100$ to $h/10{,}000$
    - Increase the flange plate thickness shown in Fig. 3 by 50%
    - Increase the steel yield strength by ~40% to Gr50 steel (see Fig. 4) in lieu of the baseline Gr36 steel

The following naming convention will be used to identify the models in this paper: *material-ar#-tr#*. The *material* term simply refers to the steel type (Gr36 or Gr50). The "tr" and "ar" labels denote the following:

- ar: aspect ratio of the stiffened web panels in the test section, equal to longitudinal panel length, *a* (measured on center between stiffeners), divided by web depth, *h*
- tr: flange-to-web thickness ratio, equal to the flange thickness, t_f, divided by web thickness, t_w

The single model that utilizes the $h/10{,}000$ initial imperfection magnitude is labeled accordingly at the end of its name to denote the reduced imperfection. The analysis results for the first group of models (Gr36-ar1-tr4, Gr36-ar1.5-tr4, and Gr36-ar3-tr4) will be presented in Section 4 of this paper. Results for the second group (Gr36-ar1-tr4-h/10,000, Gr36-ar1-tr6, and Gr50-ar1-tr4) will be presented in Section 5.

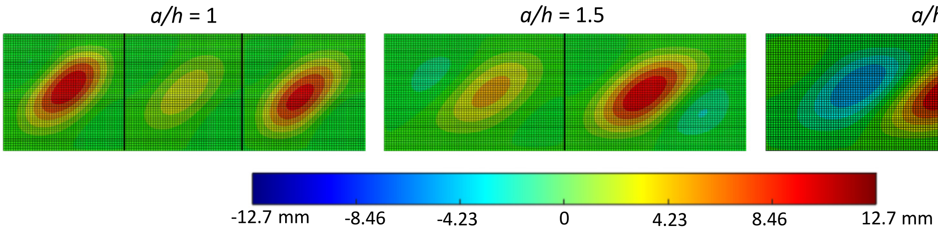

Fig. 6. Contours of first eigenmode initial imperfections in the web test section, scaled to a maximum amplitude of h/100 for the prototype girder with varying web panel aspect ratio.

4. Group 1 results: Varying panel aspect ratio

The shear load–displacement resulting from Modified Riks analysis for the first group of girder cases with varying aspect ratio are plotted in the (a) column of Fig. 7. Each case exhibits a variation of the PM-C Stage 3 response per Fig. 2, with the ar1 and ar1.5 cases showing a more gradual initial descending branch than ar3 after reaching maximum shear resistance at the onset of the web mechanism. This response is expected due to larger panel stiffness at lower aspect ratio, even after the web mechanism has formed.

To quantitatively identify the milestones within and between each stage of response, a derivative is calculated from the shear load vs. displacement curve to obtain a stiffness (k, expressed as kN/mm) vs. displacement relationship. A subsequent derivative is then calculated from the stiffness vs. displacement relationship to obtain the change in stiffness (Δk, expressed as kN/mm/mm) as a function of displacement. For this study, the values of k and Δk at each displacement increment x are simply calculated via forward difference using Matlab [38]:

$$k_x = \frac{V_{x+1} - V_x}{\delta_{x+1} - \delta_x} \tag{1}$$

$$\Delta k_x = \frac{k_{x+1} - k_x}{\delta_{x+1} - \delta_x} \tag{2}$$

Fig. 7 also includes plots of (b) stiffness, k; and (c) change in stiffness, Δk when these equations are applied to the load–displacement results from FE analysis of each model case ar1 through ar3. Each curve in Fig. 7 includes four color-coded markers that correspond to milestones V_{cr}, V_{el}, V_{m1}, and V_{m2} (which were defined previously in Section 2). Table 1 describes how each milestone was obtained from the FE model results and correlates these milestones to the onset of the web and panel mechanisms.

4.1. Evaluation of shear response stages

The shear values corresponding to each milestone are summarized in Table 2, and contour plots of the out-of-plane web deformations at each milestone are provided in Fig. 8. Contours of von Mises stresses (calculated from the total stress results from FE analysis) are plotted in Fig. 9 (ar1), Fig. 10 (ar1.5), and Fig. 11 (ar3) for each milestone at the front, middle, and back, integration points through the thickness of the web plate. Dark red saturation in these contours indicates that the steel material has exceeded its yield strength per Fig. 4. A detailed discussion of each response stage is provided in the following subsections.

4.1.1. During the elastic stage (at V_{cr})

The initial stiffness in the load–displacement plots in Fig. 7a visually appears to be quasi-linear, and previous studies such as that by Scandella et al. [29] have referred to this stage as “linear elastic”. However, the plots in Fig. 7b clearly show a progressive decrease in stiffness throughout in initial shear loading stage. It is important to note that the plate does not have constant linear stiffness during this stage because it is not perfectly flat at any stage of its response and therefore cannot respond as a membrane in pure shear. Even though the out-of-plane deformations are visually imperceptible at this milestone in Fig. 8, the initial imperfections shown previously in Fig. 6 will indeed deform via second-order bending due to shear-induced compression from the onset of shear load application. The deformed web plate therefore responds elastically prior to the onset of yielding but with reduced stiffness as the second-order bending progresses. Fig. 7c shows that the rate of stiffness change (Δk) is initially negative but small at the V_{cr} milestone; however, Δk then accelerates downward as the web panel progresses toward V_{el}.

The contour plots of von Mises stress in Figs. 9 through 11 show that the web plate is well below yield during this stage as expected. The middle integration point consistently shows low stress across the web plate for all three girder cases; however, the patterns of von Mises stress concentrations on the front and back surfaces of the ar1 and ar1.5 cases clearly show an increase in second-order bending stress at the same locations of the most significant out-of-plane deformations. The ar3 web shows much less observable increase in front/back surface von Mises stress during this stage from second-order bending due to its reduced shear stiffness versus those with shorter aspect ratio.

4.1.2. At the elastic limit (V_{el})

As shown in Fig. 8, the largest band of out-of-plane deformation at the elastic limit for the ar1 and ar1.5 cases has developed across the tension field diagonal, at the same location where second-order bending is the most severe due to compression from the opposite diagonal. The von Mises stress contours for ar1 (Fig. 9) and ar1.5 (Fig. 10) at V_{el} show that the tension field diagonal will interact with surface stresses from second-order bending to create a continuous pathway of von Mises yielding across this diagonal, particularly on the “back” surface (where second-order bending stress is tensile). The middle integration point, however, has not yet developed a yielded pathway across the tension diagonal. When the surface yield pathway becomes connected across the tension diagonal, the ar1 and ar1.5 webs both exhibit their first sudden change (i.e. downward spike) of Δk in Fig. 7c (marked with the gray square).

The von Mises stress contours for the ar1 and ar1.5 cases also show that the corners of the webs at the opposite ends of the tension field have already begun to yield across the full thickness of the web plate (i.e. at all integration points). The corners have greater planar stiffness relative to the middle region of the web panel, and the corners at the end of the tension field develop large reaction stresses as the web panel deforms in-plane under shear. As shown in Fig. 7b, the overall shear stiffness for the ar1 and ar1.5 web panels continues to decrease beyond V_{el} but still has a significant positive value as the web develops an increase of yield saturation.

For the ar3 case, the plot of out-of-plane deformation at V_{el} in Fig. 8 shows three half wavelengths with similar amplitude, and each of those wavelengths has a peanut-shaped bulge pattern in the tension diagonal direction. This web has significantly less shear resistance compared to ar1 and ar1.5 due to its larger aspect ratio, and its largest out-of-plane deformations (and, correspondingly, its most intense band of von Mises stress in Fig. 11) do not span the full corner-to-corner distance of the tension field diagonal (i.e. they come up short and terminate over the flange). The increased complexity of the deformed shape slightly alters the onset of the elastic limit milestone for ar3 (which is the highest

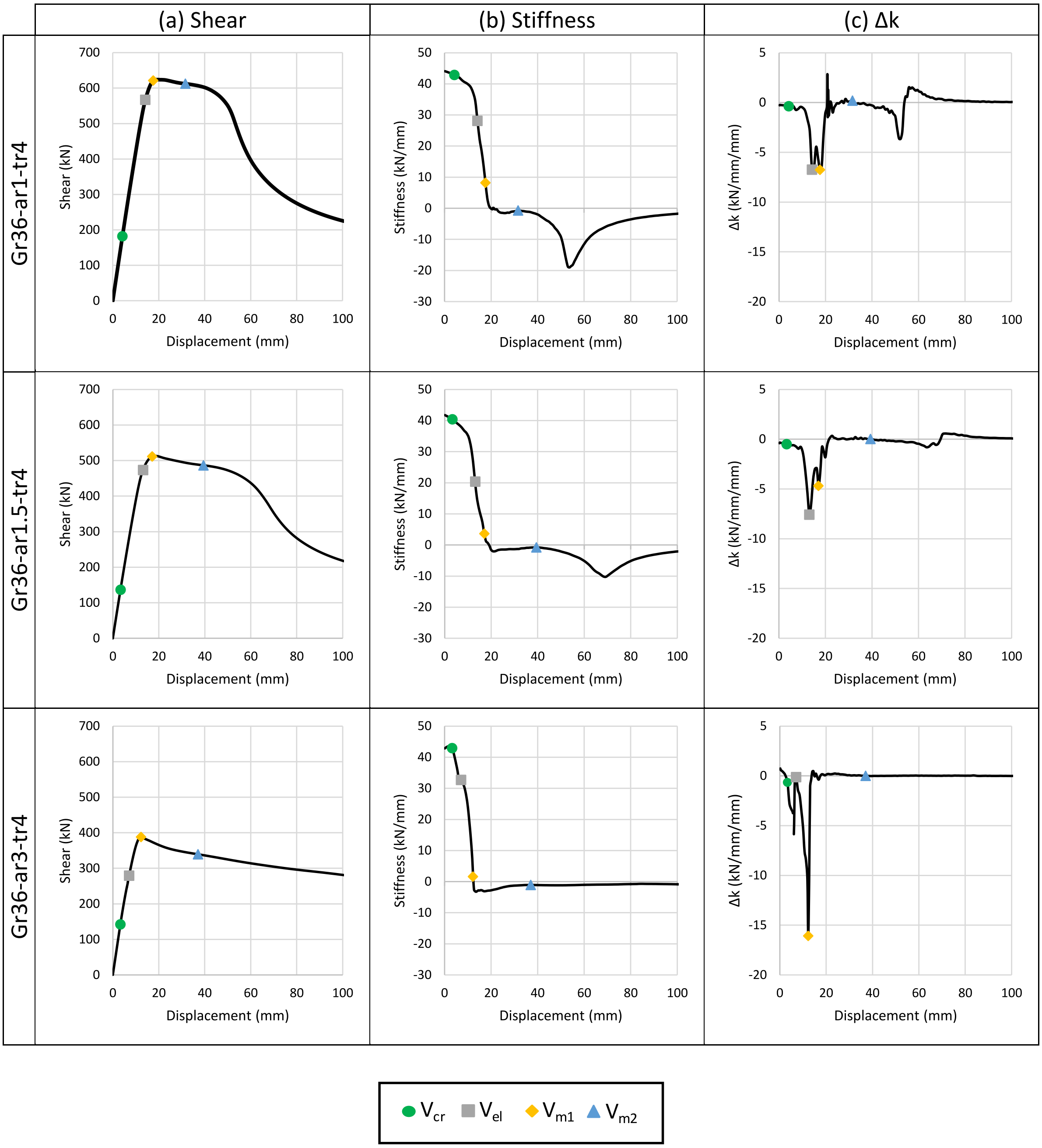

Fig. 7. Plots of FE results for the Gr36-arX-tr4 model cases with varying web panel aspect ratio: (a) shear vs. displacement, (b) stiffness vs. displacement, and (c) change in stiffness vs. displacement.

aspect ratio considered to be capable of tension field action per AISC 360-16 [5]), but the overall mechanics are still similar to ar1 and ar1.5. The von Mises contours in Fig. 11 for the ar3 case at the V_{el} milestone show that several elongated pockets of surface yielding have formed due to the interaction of tension field stresses and localized second-order bending stresses. These pockets bridge between the buckled bulge pattern in the ar3 deformed shape, thus enabling a sudden change in the ar3 plot of Δk in Fig. 7c (again marked with the gray square). Note that this is the second sudden change in Δk for ar3 — the first occurs when the complex ar3 buckled shape readjusts from its initial imperfection pattern and “settles” into the shape from which von Mises yielding then emerges.

4.1.3. At web mechanism formation (V_{m1})

At V_{m1}, all three a/h cases develop a triple-curvature deformation pattern in Fig. 8 (i.e. with three half-wavelengths) along the compression diagonal due to second-order bending of the deformed web plate. The von Mises stresses in all girder cases in Figs. 9 through 11 show full-thickness yielding (i.e. at all integration points) over a corner-to-corner band of the tension diagonal in at least one web panel. The front/back integration points show extensive von Mises yielding due to increases in both the tension field stresses and second-order bending stresses, but the web mechanism and subsequent significant loss of stiffness in Fig. 7a does not occur until a band of thru-thickness yielding has developed at the location of maximum second-order bending.

Table 1
Milestone marker definitions for plotting generalized shear response.

Milestone	Stage description	Plot marker	Method for identification from FE results
V_{cr}	During Stage 1 (Elastic Behavior)	Green dot	**From buckle analysis**: The value of V_{cr} is calculated as the first eigenmode from the preliminary "buckle" analysis of the idealized flat web to obtain imperfection patterns. **Correlations**: The V_{cr} milestone is merely used to represent a point within the initial elastic stage. V_{cr} has no correlation to any mechanical behavior from the Modified Riks analysis of a shear loaded slender web plate with realistically sized initial imperfections. Due to second-order bending of the imperfections, these webs will not demonstrate a clear buckling bifurcation and will instead undergo an initial elastic shear-displacement response.
V_{el}	End of Stage 1 (at Elastic Limit)	Gray square	**From modified Riks analysis**: The value of V_{el} is identified using von Mises stress plots and corresponds to the shear at which the web panel has developed its first connected pathway of surface yielding across the tension diagonal due to the interaction of tensile stresses with second-order bending stresses. **Correlations**: V_{el} also correlates to a sudden change or spike in the Δk vs. displacement plots from the Modified Riks analysis.
V_{m1}	End of Stage 2 (at Web Mechanism Formation)	Yellow diamond	**From modified Riks analysis**: The value of V_{m1} is identified using the von Mises stress plots and corresponds to the shear at which the web panel has developed a connected pathway of thru-thickness yielding across the tension diagonal due to the interaction of tensile stresses with second-order bending stresses. Due to this interaction, the thru-thickness yielding only emerges at thinly banded strips that coincide with the locations of maximum second-order ("bulging") stresses. **Correlations**: V_{m1} also correlates to a subsequent sudden change in the Δk vs. displacement plots from the Modified Riks analysis.
V_{m2}	During Stage 3 (Panel Mechanism)	Blue triangle	**From modified Riks analysis**: The value of V_{m2} is identified using the stiffness vs. displacement plots and corresponds to the shear at which the web panel stiffness has reached the end of a minor recovery following the onset of the web mechanism at V_{m1}. This recovery, which can be very subtle compared to the initial elastic shear stiffness of the web panel, occurs due to engagement of the flanges and stiffeners as anchorage load pathways. peak in the plot following the stiffness recovery (i.e. the end of the phase where the stiffness increases following the largest negative value). Sometimes the recovery can be very subtle. **Correlations**: V_{m2} also correlates to a widespread saturation of thru-thickness von Mises yielding from the Modified Riks analysis over the full width of the tension field diagonal. This single smeared band of thru-thickness yielding no longer shows any patterns that would correspond to second-order bending in the buckled shape.

Table 2
Summary of milestone shear loads (kN) for all six model cases.

Model case	During elastic stage (V_{cr})	Elastic limit (V_{el})	First (web) mechanism (V_{m1})	Second (panel) mechanism (V_{m2})	Maximum shear (V_{max})
Gr36-ar1-tr4	182	565	621	612	624
Gr36-ar1.5-tr4	138	472	512	487	513
Gr36-ar3-tr4	142	260	387	339	388
Gr36-ar1-tr4-h/10,000	182	596	618	612	621
Gr36-ar1-tr6	182	583	642	694	699
Gr50-ar1-tr4	182	747	820	828	830

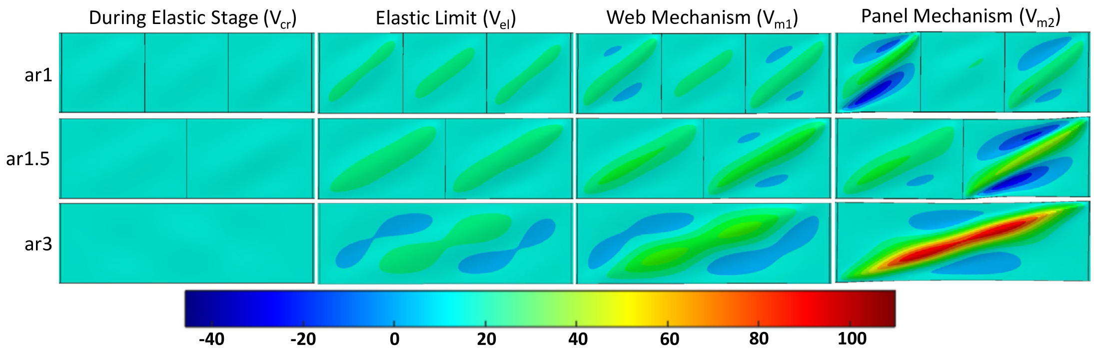

Fig. 8. Out-of-plane deformation (mm) contours from FE analyses of the Gr36-arX-tr4 model cases with varying web panel aspect ratio.

For further illustration, Fig. 12 plots the von Mises stress contours for the ar1 case at $V = 601$ kN, just before the onset of the web mechanism at $V_{m1} = 621$ kN. The front/back integration points show one or more continuous bands of von Mises yielding across the tension diagonal at locations with high second-order bending, but the mid-thickness integration point has not quite developed a fully connected band of yielding at the location of maximum second-order bending. Once that mid-thickness band develops, the shear stiffness will rapidly approach zero as shown in Fig. 7b.

The value of plastic shear (which represents yielding over the full web depth) is defined as follows per AISC 360-16 [5]:

$$V_p = \frac{1}{\sqrt{3}} F_y t_w h \tag{3}$$

and equals 960 kN and 1348 kN for the Gr36 and Gr50 model cases, respectively. When combined with the values in Table 2, the ratios of V_{m1}/V_p among the six model cases vary between 0.40 and 0.67, with smaller ar ratios having larger V_{m1}/V_p ratios. A smaller ar ratio also has a larger relative value of V_{m1}, and thus a larger V_{m1}/V_p ratio. Recall

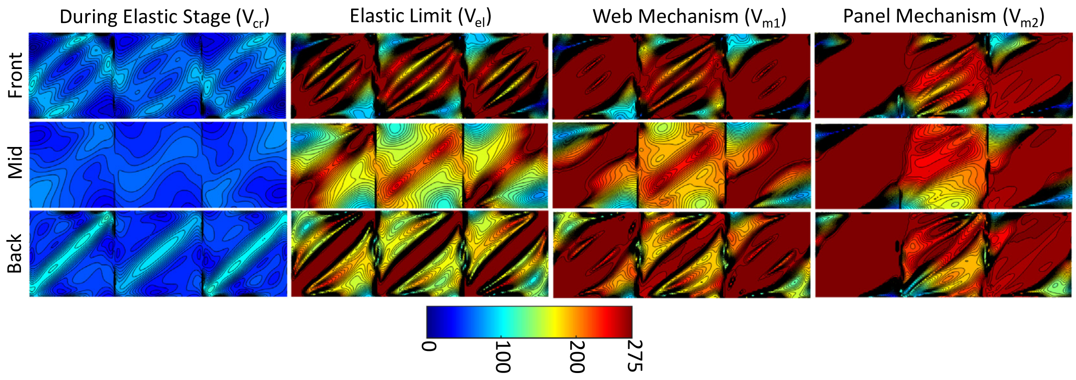

Fig. 9. Contours of von Mises stresses (MPa) at surface and mid-thickness integration points for Gr36-ar1-tr4 at several milestones of shear behavior.

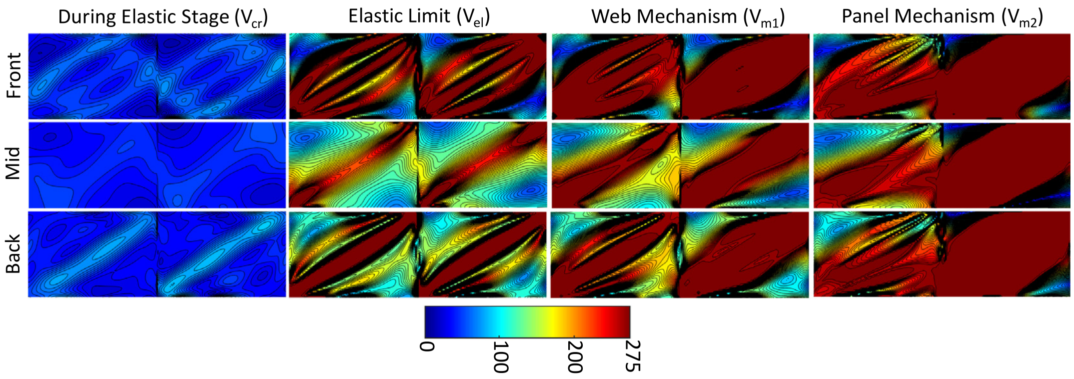

Fig. 10. Contours of von Mises stresses (MPa) at surface and mid-thickness integration points for Gr36-ar1.5-tr4 at several milestones of shear behavior.

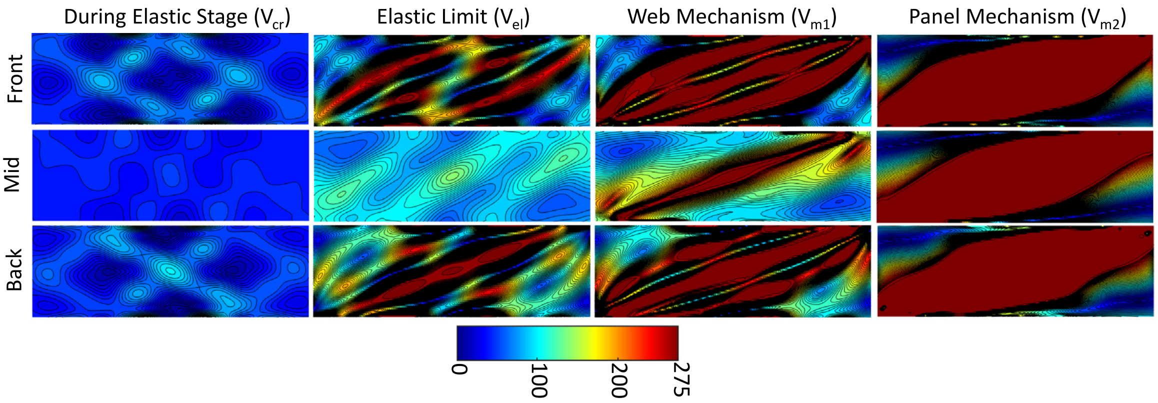

Fig. 11. Contours of von Mises stresses (MPa) at surface and mid-thickness integration points for Gr36-ar3-tr4 at several milestones of shear behavior.

that V_{m1} is defined as the shear when the web has yielded through the full thickness over a connected band across the tension diagonal — it is therefore reasonable that the V_{m1}/V_p ratio would be less than unity since the overall depth of yielding at V_{m1} is significantly less than the full depth h.

4.1.4. At panel mechanism formation (V_{m2})

None of the three girder cases considered in this section exhibited a marked increase in shear resistance after the development of the web mechanism at V_{m1} (representing a PM-C Stage 3 response per Fig. 2). For these cases, maximum shear resistance is reached just after V_{m1} (see Table 2) once the stiffness curves cross zero in Fig. 7b. Beyond that point, the ar1 and ar1.5 cases exhibit an initially gradual descending branch as the plastified web develops new anchorage pathways to the flanges and stiffeners [11] as well as to the unyielded regions of the web itself. At V_{m2}, the out-of-plane deformations in Fig. 8 due to second-order bending have intensified, and the von Mises stresses in Figs. 9 through 11 exhibit increasingly levels of thru-thickness yield saturation in at least one web panel. In particular, the von Mises yield saturation has now smeared beyond the individual bands of thru-thickness yielding that developed at the onset of the first shear mechanism into a more continuous field that begins to resemble the prominent tension field design-basis models shown previously in Fig. 1. Beyond V_{m2}, the web panel enters the descending branch toward having negligible remaining shear resistance.

4.2. Commentary on membrane stress response

As discussed earlier in this paper, most design approaches for shear resistance of slender stiffened webs in current practice [5–7] assume a wide band of tension field membrane response across the tension

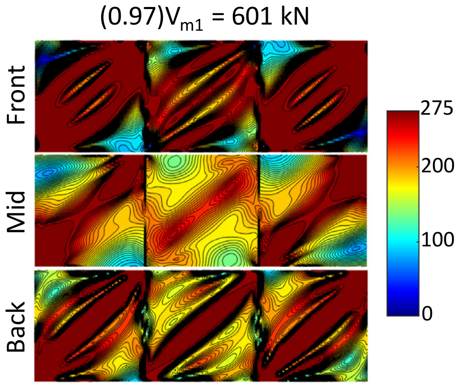

Fig. 12. Contours of von Mises stresses (MPa) at surface and mid-thickness integration points for Gr36-ar1-tr4 just prior to the development of a web mechanism.

diagonal of the web panel [8–10] as shown in Fig. 1b–d. The second-order bending behavior of the buckled web is therefore neglected, and shear resistance is calculated as a function of tension field yielding in combination with contributions from the flanges and/or intermediate stiffeners. The analysis results in the previous section clearly demonstrate the role of the compression-induced second-order bending in developing the web mechanism via stress interaction with the tension field. Closer examination of the membrane stresses from the FE analyses of these girder cases with varying web panel aspect ratio can also confirm that a web mechanism cannot be achieved via membrane effects alone. To do so, the SSAVG membrane stresses ($\sigma_{xx}, \sigma_{yy}, \tau_{xy}$) for the web were also extracted from the Modified Riks analysis results in Abaqus. These stress values, which represent the weighted average among all integration points in the shell element thickness, can then be used to calculate the principal membrane stresses (σ_1, σ_2), principal membrane stress angles (θ), and von Mises membrane stresses ($\sigma_{v,membrane}$) as follows:

$$\sigma_1, \sigma_2 = \frac{\sigma_{xx} + \sigma_{yy}}{2} \pm \sqrt{\left(\frac{\sigma_{xx} - \sigma_{yy}}{2}\right)^2 + {\tau_{xy}}^2} \tag{4}$$

$$\theta = \frac{1}{2}\tan^{-1}\left(\frac{2\tau_{xy}}{\sigma_{xx} - \sigma_{yy}}\right) \tag{5}$$

$$\sigma_{v,membrane} = \sqrt{\frac{\left(\sigma_1 - \sigma_2\right)^2 + (\sigma_2 - \sigma_3)^2 + (\sigma_3 - \sigma_1)^2}{2}} \tag{6}$$

Note that $\sigma_{v,membrane}$ calculated here is based solely on membrane stresses and is different from the von Mises stresses plotted in Figs. 9 through 12, which are based on the stresses at specific integration points though the thickness of the web plate.

Contours of membrane stresses for the ar1, ar1.5, and ar3 cases are plotted in Figs. 13, 14, and 15, respectively, at the same four milestones considered in Section 4.1. As a first observation, it is noteworthy that none of the von Mises membrane stress contours at the web mechanism milestone exhibits any dark-red yielding, which directly indicates that the onset of web plasticity is dependent on the interaction of tension field stresses with second-order bending stresses. The membrane results by themselves cannot explain why the web panel experiences a rapid and significant loss of stiffness at this milestone. The contours of maximum principal and von Mises stress both show the clear development of a tension diagonal at the V_{el} through V_{m2}, but the largest magnitudes of tension flow through narrow bands at the inflection points of the triple-curvature buckled shape of the web shown previously in Fig. 8. This is an important distinction from most prominent tension field theories, which assume a relatively uniform distribution of membrane stresses over the width of the tension diagonal. Instead, these results indicate that the membrane portion of the tension field is most intense in areas with the least amount of second-order bending. The contours of minimum principal stress are relatively uniform and do not clearly indicate the spring-like compression resistance that is provided by second-order bending in the deformed plate along the compression diagonal.

Another commonality among all the tension field action theories is that the principal stress angle becomes shallower than the initial 45° pure shear assumption as post-buckling behavior progresses and the tension field makes larger load path contributions than the compression diagonal [8–10]. Contours of principal membrane stress angles for the three girder cases considered in this section are plotted in Fig. 16 for further examination. During the elastic stage at V_{cr}, the principal membrane stress angles already have a somewhat vortexed contour and are shallower than 45°, thus indicating an early onset of tension field diagonalization as well as second-order elastic bending in the initial imperfections. The principal membrane stress angles then become progressively shallower from V_{el} through V_{m2}. At the development of the web mechanism at V_{m1}, the principal membrane stresses vary approximately between 25° to 35° in the tension field region — this variability again indicates the presence of second-order bending in the out-of-plane deformed shape. At this milestone, the angles become flatter (i.e. the shading is progressively greener in Fig. 16 web mechanism contours) as the web panel aspect ratio increases from ar1 to ar3. The magnitude of tension field action progressively decreases as aspect ratio increases due to lower panel stiffness; for the same reason, these principal angle contours indicate that panels with larger aspect ratios will develop more tension field action relative to the intensity of the compression diagonal load path. In other words, the spring-like

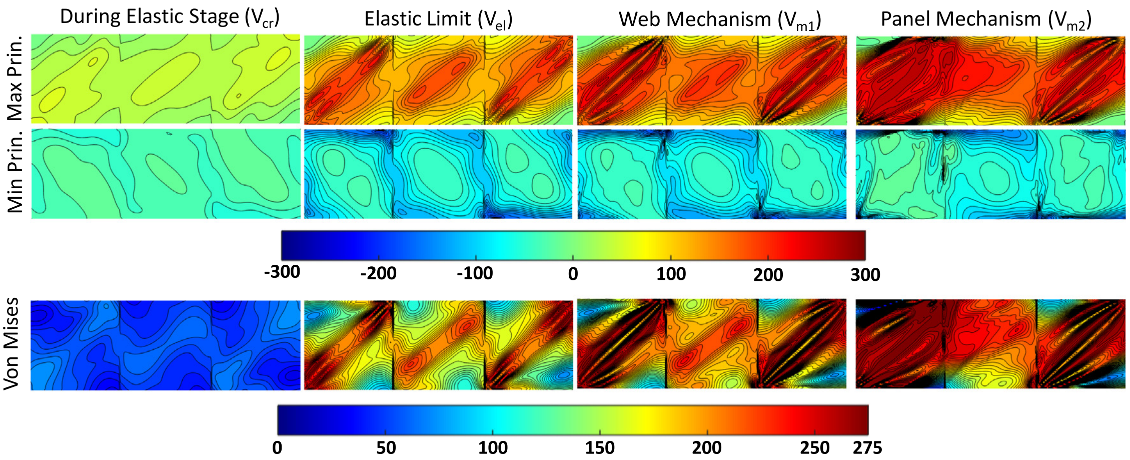

Fig. 13. Contours of membrane stresses (MPa) from FE analysis of Gr36-ar1-tr4.

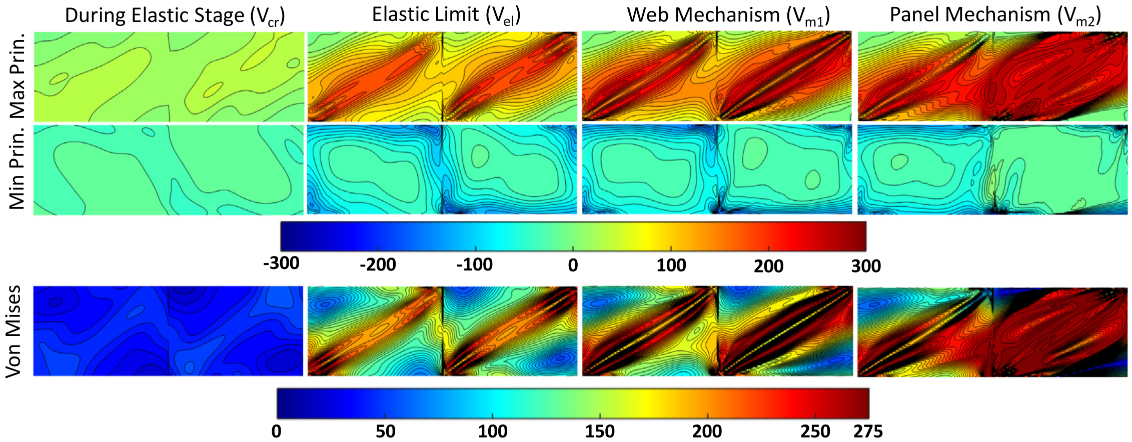

Fig. 14. Contours of membrane stresses (MPa) from FE analysis of Gr36-ar1.5-tr4.

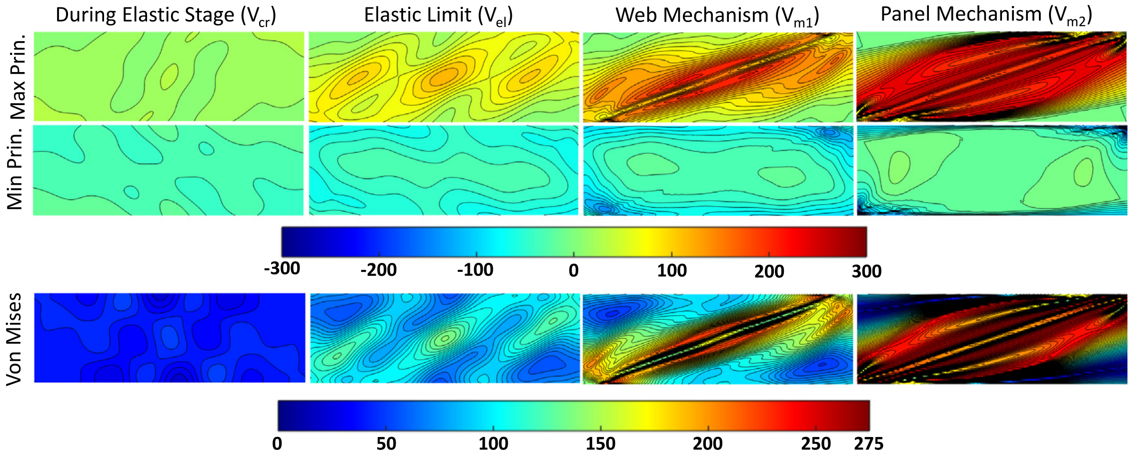

Fig. 15. Contours of membrane stresses (MPa) from FE analysis of Gr36-ar3-tr4.

second-order bending behavior in the compression diagonal becomes proportionally less engaged at larger aspect ratios (in this case, at ar3) versus the membrane response of tension field action.

5. Group 2 results: Other parametric variations

The results in Section 4 demonstrate a common mode of web mechanism formation for the prototype girder with varying aspect ratio. The same mechanics will be demonstrated in this section for the second group of model cases with ar1 to examine a decrease in initial imperfection magnitude to "nearly flat" (Gr36-ar1-tr4-$h/10{,}000$), a 50% increase in flange thickness (Gr36-ar1-tr6), and an increase in steel yield strength per Fig. 4 (Gr50-ar1-tr4). The shear load–displacement from of FE analysis (using the same procedure discussed previously in Section 2) of all ar1 cases are plotted in Fig. 17 for direct comparison. A breakout of FE results for the second group of model cases is plotted in Fig. 18, which also includes plots of stiffness and change in stiffness similar to those for the first group of model cases in Fig. 7. The same four milestones (V_{cr}, V_{el}, V_{m1}, V_{m2}) that were utilized in Section 4.1 are marked on Fig. 18 plots, and the shear values corresponding to each milestone are summarized in Table 2. Analysis results in Figs. 17 and 18a for the reduced $h/10{,}000$ initial imperfection and the Gr50 increase steel yield strength both exhibit a very similar PM-C panel mechanism response (see Fig. 2) as was shown for the Gr36-ar1-tr4 baseline model in Fig. 7a. The case with increased flange thickness experienced hardening during its panel mechanism stage (i.e. a PM-A response per Fig. 2), resulting in an 8% increase in shear resistance from V_{m1} to V_{max} (see Table 2).

5.1. Effects of decreased initial imperfection magnitude

Fig. 17 shows practically identical shear load–displacement behavior for the Gr36-ar1-tr4 models with $h/100$ and $h/10{,}000$ initial imperfection magnitudes. The contours of von Mises stresses for the $h/10{,}000$ case at the surface and mid-thickness integration points Fig. 19 show a very similar onset of yielding from V_{el} through V_{m2} as the $h/100$ contours in Fig. 9. The $h/10{,}000$ imperfection was therefore large enough to enable bands of surface yielding across the tension field diagonal (where second-order bending stresses in the deformed web are greatest) at the elastic limit, followed by thru-thickness yielding at the same location to initiate the web mechanism.

The only significant difference between the $h/100$ and $h/10{,}000$ contours is during the initial elastic stage. As would be expected, the $h/10{,}000$ case shows very little diagonalization of low-level von Mises stress at V_{cr} (indicating negligible levels of second-order bending) versus the $h/100$ case, which already shows the onset of second-order bending in its deformed shape with larger initial imperfections. Despite this, decreasing the initial imperfection magnitude to the "nearly flat" $h/10{,}000$ value produced negligible change in elastic stiffness, the subsequent web mechanism formation, or the mode of panel mechanism response. These results clearly show that the web mechanism formation (resulting from of von Mises stress interaction between the tension field diagonal and second-order bending in the compression diagonal) is not sensitive to the magnitude of initial imperfection. Upcoming work by the authors is exploring the influence of the shape of initial imperfections that deviate from the eigenmodes that were used in this study. In previous work, however, the authors showed that the

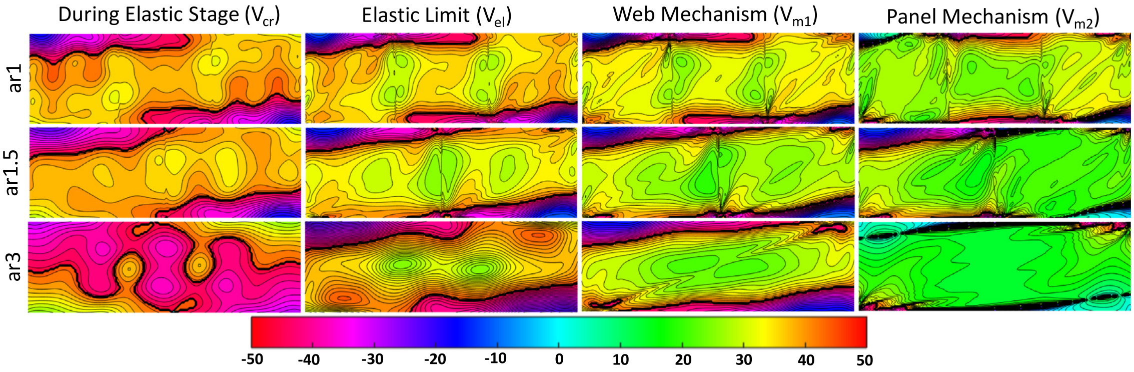

Fig. 16. Contours of principal membrane stress angles from FE analyses of the Gr36-arX-tr4 girder cases with varying web panel aspect ratio. (For interpretation of the references to color in this figure legend, the reader is referred to the web version of this article.)

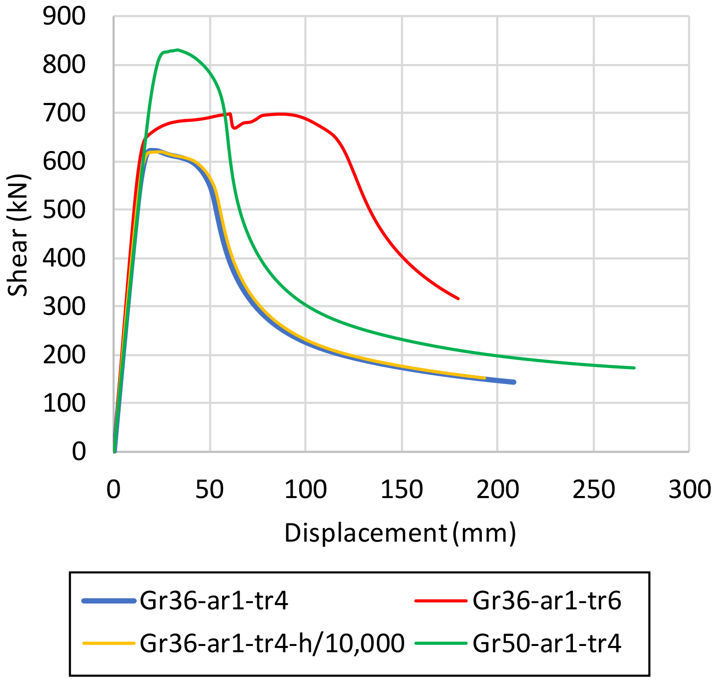

Fig. 17. Comparison of shear load vs. displacement from FE analyses for all ar1 model cases.

first eigenmode initial imperfection approach described in Section 2.3 enabled very good FE predictions [11] of the experimental results by Basler et al. [24] for the baseline cases of the prototype girder.

5.2. Effects of increased flange thickness

The Gr36-ar1-tr6 model case was developed by increasing the flange thickness of the Gr36-ar1-tr4 baseline case by 50% (from 19.05 mm to 28.575 mm). As a result, the thicker flange enabled a PM-A panel mechanism response (per Fig. 2) as shown in the shear load–displacement plots of Figs. 17 and 18a. Once the web mechanism develops, the thicker flange provides a more significant anchorage via weak-axis flexure for the load paths in the plastified web. This panel mechanism governed by flange anchorage is a feature of the ultimate shear prediction methodologies per Höglund [9] and Cardiff [10] as shown previously in Fig. 1c–d. However, Fig. 17 shows that the shear load–displacement behavior up to the development of the web mechanism for Gr36-ar1-tr6 is nearly identical to that of the baseline Gr36-ar1-tr4 case. As summarized in Table 2, the thicker flange produces only a 3% increase in V_{m1} for the tr6 case versus the tr4 case by increasing the stiffness at the top and bottom boundaries of the web panels. The contours of von Mises stress for the tr6 case at the elastic stage and elastic limit milestones are also very similar to those for the tr4 case and are therefore not included in Fig. 20 for brevity.

Fig. 20 shows a very similar pattern of von Mises yielding at V_{m1} for Gr36-ar1-tr6 as was shown in Fig. 9 for Gr36-ar1-tr4. The increased flange thickness therefore had negligible influence on the development of thru-thickness yielding along the tension diagonal due to interaction with second-order bending. The saturation of von Mises yielding across the web panels is also similar at V_{m2} when comparing the leftmost panel in the tr4 case with both end panels in the tr6 case. When the panel mechanism develops, the enhanced flange anchorage in the tr6 case therefore enables a more symmetric saturation of yielding within the two end panels. Beyond V_{m2}, the tr6 load–displacement plot in Fig. 18a shows a slight dip in shear resistance (and a sudden change in stiffness in Fig. 18b–c) until the plastified end panels begin to redistribute load to the center panel, which is slightly less yielded at this point. The thicker flange provides enhanced bridging between the panels, thus enabling this load transfer after the end panels have significantly yielded. Together, the three panels develop a slight amount of additional positive hardening until the center panel also develops a widespread saturation of thru-thickness von Mises yielding at maximum shear V_{max} in Fig. 20. V_{max} in this case therefore coincides with the

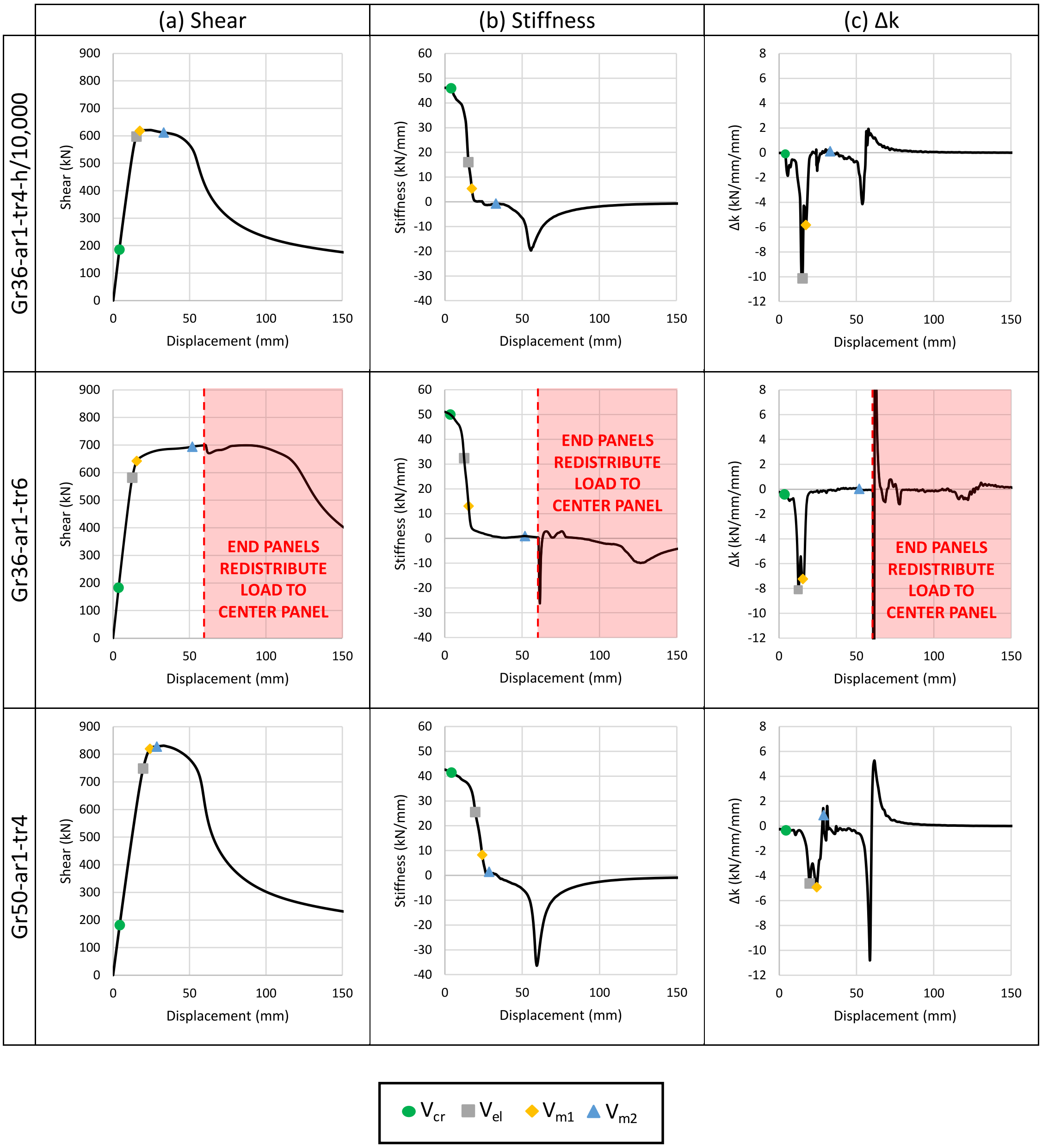

Fig. 18. Plots of FE results for the Group 2 girder model cases: (a) shear vs. displacement, (b) stiffness vs. displacement, and (c) change in stiffness vs. displacement.

development of a third mechanism in which all three web panels have become plastified, thus initiating the descending branch.

In summary, the Gr36-ar1-tr6 results show that the effects of flange anchorage for the tension field is most pronounced after the web mechanism has developed. The flanges stiffen the top and bottom of the web panel against in-plane and out-of-plane deformation, but they have little influence otherwise on the development of thru-thickness von Mises yielding due to the interaction of the tension field diagonal with second-order bending from the compression diagonal. The maximum shear state reached during a PM-A response will occur as a much larger displacement versus that at V_{m1} but with only a modest (~10%) gain in shear resistance (see Table 2). Additionally, the onset of a PM-A maximum shear state is governed not only by the available weak-axis flexural stiffness of the flange but also by the progression of yielding via load transfer between neighboring web panels.

In previous work, the authors also showed that load redistribution to the intermediate stiffeners via axial compression would become more pronounced during the panel mechanism stage after exceeding V_{m1} [11]. The sizing of the stiffeners can therefore influence the shape of the Stage 3 response. Up to V_{m1}, however, the stiffeners were primarily engaged in out-of-plane bending to define the web panelization. The sizing of the stiffeners was therefore shown to have negligible impact on the value of V_{m1} and the overall shear-displacement response through Stages 1 and 2, as long as they were adequately sized to provide out-of-plane stiffening [11]. The value of V_{m1} at the web mechanism formation could therefore be considered as a reliable design-basis shear load since it is not heavily dependent on the stiffeners, flanges, or neighboring web panels for load redistribution.

5.3. *Effects of increased steel yield strength*

Increasing the steel yield strength by 40% from Gr36 to Gr50 per Fig. 4 produced a 24% increase in the value of V_{m1} (see Table 2). However, the PM-C shapes of the shear load–displacement curves in Figs. 17 and 18a are very similar since the two model cases share the exact same geometry (including initial imperfections). The evolution of von Mises stress contours in Fig. 21 for the Gr50-ar1-tr4 case is also very similar to those in Fig. 9 for the Gr36-ar1-tr4 case. Essentially, the

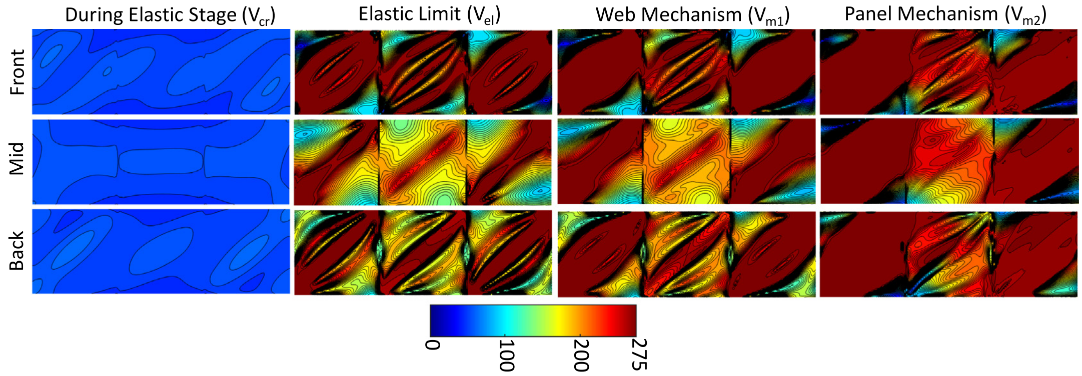

Fig. 19. Contours of von Mises stresses (MPa) at surface and mid-thickness integration points for Gr36-ar1-tr4-h/10,000 at several milestones of shear behavior.

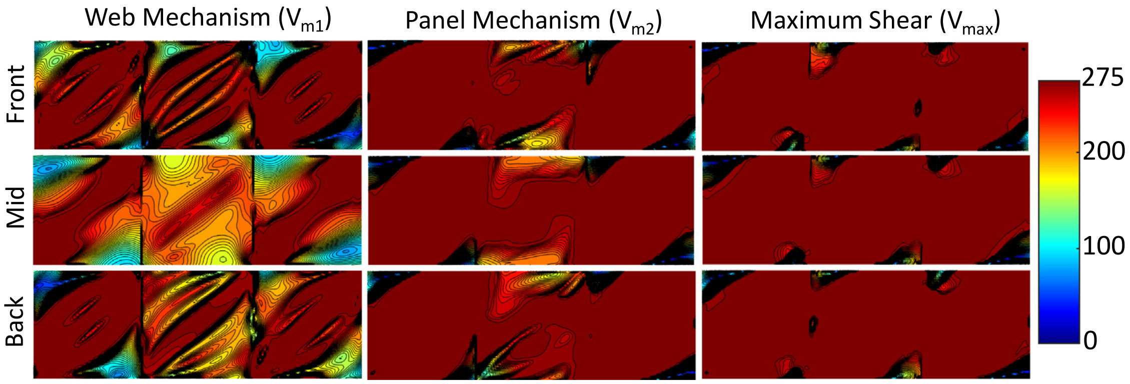

Fig. 20. Contours of von Mises stresses (MPa) at surface and mid-thickness integration points for Gr36-ar1-tr6 at several milestones of shear behavior.

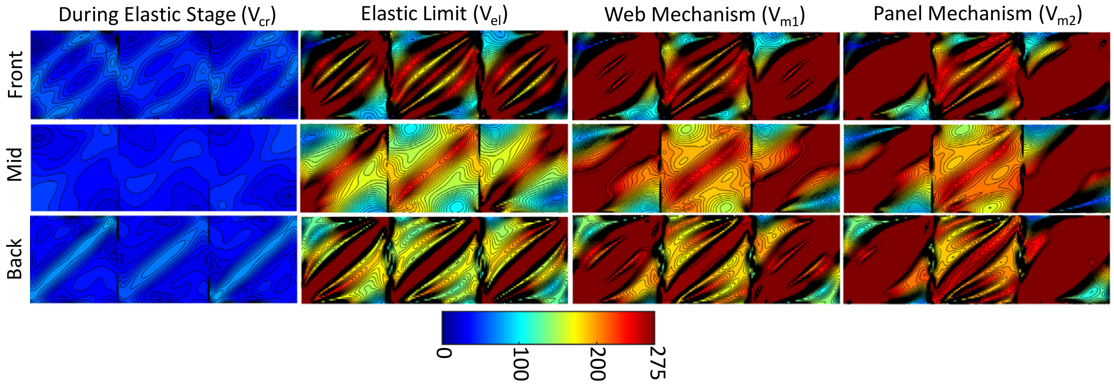

Fig. 21. Contours of von Mises stresses (MPa) at surface and mid-thickness integration points for Gr50-ar1-tr4 at several milestones of shear behavior.

change in steel grade had no influence on the mode of web mechanism formation and panel mechanism behavior. It is therefore reasonable to expect that observations and conclusions made regarding the web shear mechanics for the Gr36 girder cases can be applied to girders that utilize higher strength steel grades.

6. Selecting a design-basis shear strength

Code-based predictions of nominal shear strength for each model case per Chapter G of AISC 360-16 [5] and Section 5 of Eurocode 3, Part 1-5 [7] are summarized in Table 3. The equations and procedures for these calculations both account for tension field action up to ar3 and are detailed in the appendix of a previous paper by the authors [11] (and therefore not reproduced here for brevity). When calculating the web contribution to shear resistance, both design models apply a semi-empirical reduction to the yield strength of a flat web in pure shear, and the reduction factors rely on web shear buckling coefficients that are a function of theoretical elastic stability. However, none of the web panels modeled in this study (based upon the seminal tests which formed the initial basis for tension field theory) undergo a sudden buckling bifurcation under pure shear due to the presence of initial imperfections. Note that the AISC 360–16 predictions of web shear resistance (V_n) are unaffected by the changes in flange thickness because they are based on Basler's tension field model [8], which neglects any flange contributions. The EC3 prediction of web shear resistance ($V_{b,Rd}$), however, directly accounts for a contribution from the flanges ($V_{bf,Rd}$) in addition to that of the buckled web ($V_{bw,Rd}$), based on Höglund's prediction model [9]. Neither prediction accounts for any change in initial imperfection and therefore produce the same value for the $h/100$ and $h/10{,}000$ cases.

Table 3
Comparison of numerical results with code-based predictions of shear resistance (kN) for all six model cases.

Model case	FE model results		AISC 360-16 [5] predictions			EC3, Part 1–5 [7] predictions		
	$V_{m1,FE}$	$V_{max,FE}$	V_n	$V_n/V_{m1,FE}$	$V_n/V_{max,FE}$	$V_{b,Rd}$	$V_{b,Rd}/V_{m1,FE}$	$V_{b,Rd}/V_{max,FE}$
Gr36-ar1-tr4	621	624	640	1.03	1.03	474	0.76	0.76
Gr36-ar1.5-tr4	512	513	513	1.00	1.00	407	0.79	0.79
Gr36-ar3-tr4	387	388	323	0.83	0.83	351	0.91	0.90
Gr36-ar1-tr4-h/10,000	618	621	640	1.04	1.03	474	0.77	0.76
Gr36-ar1-tr6	642	699	640	1.00	0.92	560	0.87	0.80
Gr50-ar1-tr4	820	830	921	1.12	1.11	621	0.76	0.75

The values of V_n per AISC are very close to both $V_{m1,FE}$ and $V_{max,FE}$ (within 4%) for all Gr36 cases with ar1 or ar1.5 – this is expected because AISC's Basler-based prediction model was developed using those cases as its original basis [5,8]. Both of those model cases exhibited a PM-C response per Fig. 2, and neither experienced any marked increase in shear resistance as a result of load redistribution to the flanges, stiffeners, or adjacent web panels during the panel mechanism stage. For Gr36-ar3-tr4, the AISC prediction becomes increasingly conservative versus the FE results. For Gr36-ar1-tr6, the AISC prediction agrees well with $V_{m1,FE}$ and does not account for the 9% increase (i.e. a PM-A response) in shear resistance to $V_{max,FE}$ following the formation of the web mechanism. For the Gr50 case, the AISC prediction becomes slightly more unconservative as it attempts to account for the increase in steel yield strength. Again, the AISC approach was originally formulated for Gr36 steel, and it uses coefficients based on elastic buckling that do not necessarily account for the true onset of the web mechanism or panel mechanism as demonstrated in this study.

The values of $V_{b,Rd}$ per EC3 for the Gr36 cases are ∼25% conservative compared to the FE results for all ar1-tr4 cases regardless of steel grade. The EC3 predictions trend closer to the FE results as the aspect ratio increases (Gr36-ar1.5-tr4, Gr36-ar3-tr4) or when the flange thickness is increased (Gr36-ar1-tr6). The EC3 prediction explicitly accounts for a flange contribution, which becomes more significant as the in-plane shear stiffness of the web plate decreases (e.g. with increased aspect ratio) or with increases in the flange's torsional and flexural stiffnesses (e.g. with increased flange-to-web thickness ratio).

Overall, the code-based predictions show inconsistent agreement with V_{m1} and V_{max} across all six of the model cases, due to the fact that the mechanical formulation of the code-based models is generally inconsistent with the true onset of the web mechanism followed by the engagement of the panel mechanism. The results of this study indicate that the mechanical basis for predicting shear strength in a web with realistic initial imperfections should be correlated to the onset of the web mechanism under the combined stresses of the tension diagonal and second-order compression-driven bending, rather than to the elastic stability of an unrealistically idealized flat web plate. It would therefore be appropriate to select the web mechanism limit V_{m1} per Fig. 2 as a mechanically consistent design-basis shear resistance for stiffened web panels that develop tension field action. Any potential hardening increases in shear resistance beyond V_{m1} to a higher maximum shear strength (i.e. via a PM-A or PM-B response per Fig. 2) are modest compared to the value of V_{m1}, occur at large displacements, and are heavily dependent on load redistribution from the plastified web panel to the flanges, stiffeners, and/or neighboring web panels.

7. Summary and conclusions

The results of this numerical investigation have demonstrated that slender webs in pure shear (in this case, for a plate girder prototype per Basler et al. [11,24] with a slenderness ratio of 267) will exhibit a 3-stage response regardless of panel aspect ratio, flange thickness, steel grade, or initial imperfection magnitude. After an initial elastic response (Stage 1), a post-buckling "web" mechanism will form (Stage 2) due to the interaction of tension field stresses with compression-induced second-order bending stresses in the deformed shape. The web mechanism (which initiates a significant loss of shear stiffness) is achieved at milestone shear load V_{m1}, which marks the end of Stage 2. At that point, the web plate has developed corner-to-corner bands of thru-thickness von Mises yielding across the tension diagonal due to the interaction of the tension field with locations of maximum second-order bending stress. The increasingly plastified web then develops a "panel" mechanism (Stage 3) in which load is redistributed to its boundary elements, namely the flanges and stiffeners. During this stage, the web panel experiences large permanent deformation (both in-plane due to shear and out-of-plane due to second-order bulging of the buckled plate) as the web develops a widespread saturation of thru-thickness von Mises yielding across its tension field diagonal and into the bounding elements.

It should be noted that the results of FE analysis in this study do, in fact, confirm that tension membrane effects become increasingly dominant versus compression membrane effects to create a "rotated stress" field, as posited by conventional theories for tension field action [9]. However, the compression resistance in the web is not primarily engaged via membrane effects; rather, the spring-like action of the buckled shape in second-order bending provides the primary mode of resistance in the compression diagonal. Most code-based predictions for calculating shear resistance of slender webs [5–7] as well as the mechanical theories upon which they are based [8–10] currently neglect compression-induced second-order bending in the deformed web and rely almost exclusively on some variant of tension field membrane response.

Several conclusions can be made from the results of this study:

- The value of maximum shear resistance for a given configuration of a stiffened web panel is sensitive to the relative sizing of the web panel (in terms of slenderness, thickness, and aspect ratio) versus its boundary elements (particularly the thickness and width of the flanges and intermediate stiffeners). The panel mechanism may exhibit a hardening response with small yet positive stiffness if the flanges and stiffeners are adequately robust (enabling up to a ∼10% increase in shear resistance beyond V_{m1} for some cases considered in this study). If the boundary elements cannot provide adequate anchorage support, then the panel mechanism will be unable to support hardening and will instead exhibit a descending branch of negative stiffness toward eventual shear failure. In that case, V_{m1} at the formation of the web mechanism would be synonymous with the maximum shear resistance.
- Due to the influence of boundary element sizing on the panel mechanism response, the maximum shear resistance can occur either before or after the onset of large permanent deformations at reduced stiffness. It is therefore not prudent to simply specify maximum shear resistance as a generalized target within the context of plastic limit state design. Instead, the web mechanism shear load V_{m1} can provide a more pertinent design limit because it consistently marks the initiation of a significant loss of stiffness before the development of large permanent deformations, regardless of web panel configuration.
- The value of V_{m1} from FE analysis of the six model cases in this study equaled 0.40 to 0.67 times the value of V_p (i.e. the plastic value for full depth yielding of the web in shear). As expected,

smaller web panel aspect ratios demonstrated larger V_{m1}/V_p ratios, thus achieving a higher utilization of the web's overall shear yield capacity prior to the onset of the web mechanism.
- As expected, the shear load at V_{m1} increased with steel yield strength (though not proportionally). An increased flange thickness enabled only a slight increase in V_{m1} by providing enhanced torsional and flexural stiffening at the top and bottom edges of the web panel. The influence of intermediate stiffener sizing on the development of the web and panel mechanisms is addressed in the authors' previous work [11].

CRediT authorship contribution statement

Kevin E. Augustyn: Writing – original draft, Visualization, Validation, Software, Methodology, Investigation, Formal analysis, Conceptualization. **Spencer E. Quiel:** Writing – review & editing, Visualization, Supervision, Resources, Project administration, Methodology, Funding acquisition, Conceptualization. **Maria E.M. Garlock:** Writing – review & editing, Supervision, Project administration, Methodology, Funding acquisition.

Declaration of competing interest

The authors declare the following financial interests/personal relationships which may be considered as potential competing interests: Spencer Quiel reports that financial support was provided by National Science Foundation. Maria Garlock reports that financial support was provided by National Science Foundation.

Data availability

Data will be made available on request.

Acknowledgments

This research was sponsored by the National Science Foundation (NSF), United States of America under grants CMMI-1662886 and CMMI-1662964. All opinions expressed in this paper are the authors' and do not necessarily reflect the policies and views of NSF.

References

[1] D.R. Hingnekar, A.Y. Vyavahare, Mechanics of shear resistance in steel plate girder: Critical review, J. Struct. Eng. 146 (2020) 03120001, http://dx.doi.org/10.1061/(ASCE)ST.1943-541X.0002484.

[2] D.W. White, M.G. Barker, Shear resistance of transversely stiffened steel I-Girders, J. Struct. Eng. 134 (2008) 1425–1436, http://dx.doi.org/10.1061/(ASCE)0733-9445(2008)134:9(1425).

[3] A.W. Davies, D.S.C. Griffith, Shear strength of steel plate girders, Proc. Inst. Civ. Eng. Struct. Build. 134 (1999) 147–157, http://dx.doi.org/10.1680/istbu.1999.31381.

[4] J.D. Glassman, M.E. Moreyra Garlock, A compression model for ultimate postbuckling shear strength, Thin-Walled Struct. 102 (2016) 258–272, http://dx.doi.org/10.1016/j.tws.2016.01.016.

[5] AISC, Specification for Structural Steel Buildings (AISC 360-16), American Institute of Steel Construction, Chicago, IL, 2016.

[6] AASHTO, AASHTO LRFD Bridge Design Specifications, eighth ed., American Association of State Highway and Transportation Officials, Washington, D.C., 2017.

[7] CEN, EN 1993-1-5:2006 Eurocode 3: Design of Steel Structures - Part 1-5: Plated Structural Elements, European Committee for Standardization, Brussels, Belgium, 2009.

[8] K. Basler, Strength of plate girders in shear, J. Struct. Div. 87 (1961) 151–180.

[9] T. Höglund, Shear buckling resistance of steel and aluminium plate girders, Thin-Walled Struct. 29 (1997) 13–30, http://dx.doi.org/10.1016/S0263-8231(97)00012-8.

[10] D.M. Porter, K.C. Rockey, H.R. Evans, The collapse behaviour of plate girders loaded in shear, Struct. Eng. 53 (1975) 313–325.

[11] K.E. Augustyn, S.E. Quiel, M.E.M. Garlock, Post-buckling shear resistance of slender girder webs: Stiffener participation and flange contributions, J. Construct. Steel Res. 190 (2022) 107117, http://dx.doi.org/10.1016/j.jcsr.2021.107117.

[12] P.Y. Wang, P.M. Masungi, M.E.M. Garlock, S.E. Quiel, Postbuckling mechanics in slender steel plates under pure shear: A focus on boundary conditions and load path, Thin-Walled Struct. 169 (2021) 108448, http://dx.doi.org/10.1016/j.tws.2021.108448.

[13] C.H. Yoo, S.C. Lee, Mechanics of web panel postbuckling behavior in shear, J. Struct. Eng. 132 (2006) 1580–1589.

[14] M. Xie, J.C. Chapman, Design of web stiffeners: axial forces, J. Construct. Steel Res. 59 (2003) 1035–1056, http://dx.doi.org/10.1016/S0143-974X(02)00115-3.

[15] S.C. Lee, C.H. Yoo, D.Y. Yoon, Behavior of intermediate transverse stiffeners attached on web panels, J. Struct. Eng. 128 (2002) 337–345, http://dx.doi.org/10.1061/(ASCE)0733-9445(2002)128:3(337).

[16] G.S. Stanway, J.C. Chapman, P.J. Dowling, Behaviour of a web plate in shear with an intermediate stiffener, Proc. Inst. Civ. Eng. Struct. Build. 99 (1993) 327–344, http://dx.doi.org/10.1680/istbu.1993.24354.

[17] S.C. Lee, D.S. Lee, C.H. Yoo, Further insights into postbuckling of web panels. I: Review of flange anchoring mechanism, J. Struct. Eng. 135 (2009) 3–10, http://dx.doi.org/10.1061/(ASCE)0733-9445(2009)135:1(3).

[18] S.C. Lee, D.S. Lee, C.S. Park, C.H. Yoo, Further insights into postbuckling of web panels. II: Experiments and verification of new theory, J. Struct. Eng. 135 (2009) 11–18, http://dx.doi.org/10.1061/(ASCE)0733-9445(2009)135:1(11).

[19] S. Timoshenko, J.M. Gere, Theory of Elastic Stability, second ed., Dover ed., Dover Publications, Mineola, N.Y, 2009.

[20] S.C. Lee, C.H. Yoo, Experimental study on ultimate shear strength of web panels, J. Struct. Eng. 125 (1999) 838–846, http://dx.doi.org/10.1061/(ASCE)0733-9445(1999)125:8(838).

[21] S.C. Lee, C.H. Yoo, Strength of plate girder web panels under pure shear, J. Struct. Eng. 124 (1998) 184–194, http://dx.doi.org/10.1061/(ASCE)0733-9445(1998)124:2(184).

[22] M.E.M. Garlock, S.E. Quiel, P.Y. Wang, J. Alós-Moya, J.D. Glassman, Postbuckling mechanics of a square slender steel plate in pure shear, Eng. J.-Am. Inst. Steel Constr. 56 (2019) 27–46.

[23] K. Basler, B.T. Yen, J.A. Mueller, B. Thurlimann, Web Buckling Tests on Welded Plate Girders: Overall Introduction and Part 1: The Test Girders, Lehigh University, Bethlehem, PA, 1960.

[24] K. Basler, B.T. Yen, J.A. Mueller, B. Thurlimann, Web Buckling Tests on Welded Plate Girders Part 3: Tests on Plate Girders Subjected to Shear, Lehigh University, Bethlehem, PA, 1960.

[25] K. Rockey, G. Valtinat, K. Tang, The design of transverse stiffeners on webs loaded in shear - An ultimate load approach, Proc. Inst. Civ. Eng. 71 (1981) 1069–1099, http://dx.doi.org/10.1680/iicep.1981.1757.

[26] K.H. Tang, H.R. Evans, Transverse stiffeners for plate girder web - an experimental study, J. Construct. Steel Res. 4 (1984) 253–280, http://dx.doi.org/10.1016/0143-974X(84)90002-6.

[27] A. Azizinamini, J.B. Hash, A.J. Yakel, R. Farimani, Shear capacity of hybrid plate girders, J. Bridge Eng. 12 (2007) 535–543, http://dx.doi.org/10.1061/(ASCE)1084-0702(2007)12:5(535).

[28] T. Hansen, Post-buckling strength of plate girders subjected to shear - experimental verification, Steel Constr. 11 (2018) 65–72, http://dx.doi.org/10.1002/stco.201710035.

[29] C. Scandella, M. Neuenschwander, K.M. Mosalam, M. Knobloch, M. Fontana, Structural behavior of steel-plate girders in shear: Experimental study and review of current design principles, J. Struct. Eng. 146 (2020) 04020243, http://dx.doi.org/10.1061/(ASCE)ST.1943-541X.0002804.

[30] A. Gomez, Web Out-of-Straightness in Plate Girders: Methodology for Measurements and Effects on Shear Capacity (Master's Thesis), Princeton University, 2020.

[31] K.C. Rockey, M. Skaloud, The ultimate load behaviour of plate girders loaded in shear, Struct. Eng. 50 (1972) 29–47.

[32] J. Brnic, M. Canadija, G. Turkalj, D. Lanc, Structural steel ASTM A709—Behavior at uniaxial tests conducted at lowered and elevated temperatures, short-time creep response, and fracture toughness calculation, J. Eng. Mech. 136 (2010) 1083–1089, http://dx.doi.org/10.1061/(ASCE)EM.1943-7889.0000152.

[33] Dassault Systemes Simulia Corp., Abaqus/Standard 2020, 2020, https://www.3ds.com/products-services/simulia/products/abaqus/.

[34] Dassault Systemes Simulia Corp., Abaqus Analysis User's Guide, 2015, http://130.149.89.49:2080/v2016/books/usb/default.htm.

[35] A. Ghadami, V. Broujerdian, Shear behavior of steel plate girders considering variations in geometrical properties, J. Construct. Steel Res. 153 (2019) 567–577, http://dx.doi.org/10.1016/j.jcsr.2018.11.009.

[36] E. Maiorana, C. Pellegrino, C. Modena, Imperfections in steel girder webs with and without perforations under patch loading, J. Construct. Steel Res. 65 (2009) 1121–1129, http://dx.doi.org/10.1016/j.jcsr.2008.10.007.

[37] B. Johansson, M. Veljkovic, Steel plated structures, Prog. Struct. Eng. Mater. 3 (2001) 13–27, http://dx.doi.org/10.1002/pse.59.

[38] The MathWorks, Inc., MATLAB and Statistics Toolbox, Natick, Massachussetts, 2017.